

DETERMINATION OF FLOW REGIMES IN BUBBLE COLUMNS USING CFD

A Thesis

**Submitted of the College of Engineering
Of Nahrain University in Partial
Fulfillment of the Requirements for
the Degree of Master of Science in
Chemical Engineering**

by

**Rana Rasool Jaleel
(B.Sc. in Chemical Engineering 2005)**

Muharram

1430

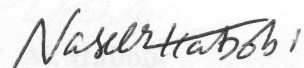
January

2009

Certification

I certify that this thesis entitled “ **DETERMINATION OF FLOW REGIMES IN BUBBLE COLUMNS USING CFD** ” was prepared by **Rana Rasool Jaleel** under my supervision at Nahrain University/College of Engineering in partial fulfillment of the requirements for the degree of Master of Science in Chemical Engineering.

Signature:



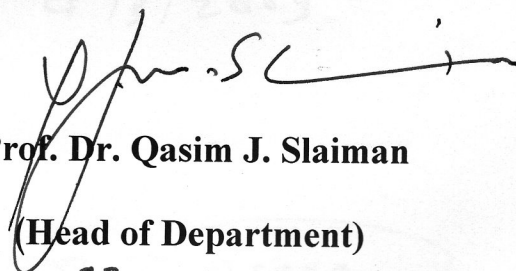
Name:

Dr. Naseer A. AL. Habobi
(Supervisor)

Date:

19 / 2 / 2009

Signature:



Name:

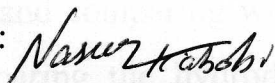
Prof. Dr. Qasim J. Slaiman
(Head of Department)

Date:

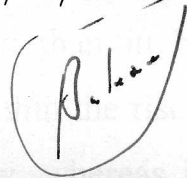
23 / 4 / 2009

Certificate

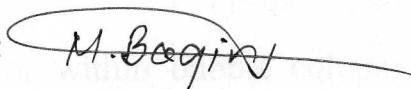
We certify, as an examining committee, that we have read this thesis entitled "**DETERMINATION OF FLOW REGIMES IN BUBBLE COLUMNS USING CFD**", examined the student **Rana Rasool Jaleel** in its content and found it meets the standard of thesis for the degree of Master of Science in Chemical Engineering.

Signature: 
Name: **Dr. Naseer Al. Habobi**
(Supervisor)

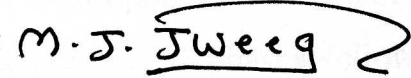
Date: 19/2/2009

Signature: 
Name: **Ass. Prof. Dr. Balasim Ahmed Abid**
(Member)

Date: 19/2/2009

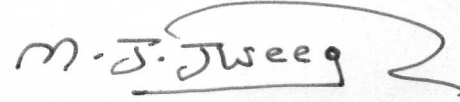
Signature: 
Name: **Dr. Mohammed Baqer M.S. Al-Shadeedi**
(Member)

Date: 04/03/2009

Signature: 
Name: **Prof. Dr. Muhsin J. Jweeg**
(Chairman)

Date: 4/3/2009

Approval of the College of Engineering

Signature: 
Name: **Prof. Dr. Muhsin J. Jweeg**
(Dean)

Date: 25/3/2009

ABSTRACT

Computational fluid dynamics (CFD) simulation, deals with the solution of fluid dynamic equations on digital computers, requiring relatively few restrictive assumptions and thus giving a complete description of the hydrodynamics of bubble columns. This detailed predicted flow field gives an accurate insight to the fluid behaviors.

3D simulation computational fluid dynamics (CFD) is applied using ANSYS-CFX Euler-Euler model to measure the hydrodynamic of an airlift reactor, and comparing with experimental data of Baten *et. al.*, (1999). Also by comparing the hydrodynamics of airlift reactor within bubble column reactor, of air/water and in the homogeneous bubble flow regime, it can be noticed that the liquid circulation velocities are more significant in the airlift configuration than in bubble columns, leading to significantly lower gas holdups. Within the riser of the airlift, the gas and liquid phases are virtually in plug flow, whereas in bubble column the gas and liquid phases follow parabolic velocity distribution. The transition regime appears at high superficial gas velocity in airlift reactors because of its ability to operate in the homogeneous bubble flow regime till much higher superficial gas velocities.

CONTENTS

Abstract	I
Contents	II
Notations	IV
List of Tables	VI
List of Figures	VII
Chapter One: Introduction	
1.1 Bubble Column	1
1.2 Computational Fluid Dynamics (CFD)	2
1.2.2 Performance of CFD	4
1.2.3 Flow & Mixing Applications of CFD	6
1.2.4 Parameters of CFD	6
1.3 Aim of the work	7
Chapter Two: Literature Survey	
2.1 Gas Holdup	8
2.2 Axial Liquid Velocities	10
2.3 Numeric Simulation in Fluids	11
2.4 Transition Regime	15
Chapter Three: Theoretical Aspect	
3.1 Hydrodynamics in Bubble Column and Airlift Reactor	18
3.2 Factors Influencing Hydrodynamics of Bubble Column Reactors	18
3.3 Flow Regime	22
3.3.1 Homogenous Flow	22
3.3.2 Heterogeneous Flow	23
3.3.2.1 Churn-Turbulent Flows	23
3.3.2.2 Slug Flow	23

3.4 Bubble Formation	24
3.5 Bubble Coalescence and Break-up	24
3.6 Bubbles Motion	26
3.7 Relationship between the Riser and Downcomer Gas Holdup in Airlift Reactors	26
3.8 Axial Liquid Velocity	32
3.9 Transition Regime	33
Chapter Four: Results and Discussion	
4.1 Computational Fluid Dynamics (CFD) Simulation	36
4.2 Computing Technology	36
4.3 Development of CFD Model	37
4.4 Simulation Results	39
4.5 Mechanism of Flow in Airlift Reactors	46
4.6 Radial Distribution	49
4.7 Transition Velocity	51
4.8 Transition Regime Identification Using the Drift Flux Plot	52
4.9 Comparisons between the Hydrodynamics in the Airlift Reactor with Bubble Columns	53
Chapter Five: Conclusions and Recommendation for Future Work	
5.1 Conclusions	58
5.2 Recommendations for future work	59
References	60
Appendix "A"	A-1
Appendix "B"	B-1
Appendix "C"	C-1

NOTATIONS

Roman letters

A	Cross-sectional area	m^2
a_L	Specific gas-liquid interfacial area	m^{-1}
d_I	Constant	-
d_B	Bubble diameter	m
D_T	Column diameter	m
F_s	Flow strength	m^3/s
g	Acceleration due to gravity	m/s^2
H	Vertical height	m
L_I	Equals D_T whichever is smaller	m
Q	Flow rate	m^3/s
R	Radius of bubble column	m
r	Radial coordinate	m
U	Superficial velocity	m/s
u_{br}	Rising velocity of isolated bubble	m/s
u_z	z-Component of liquid velocity	m/s
V	Linear velocity or axial velocity	m/s
W	Width of the column	m
z	Vertical coordinates	m
Z	Vertical distance above the sparger	m

Greek letters

ε	Phase holdup	-
$\bar{\varepsilon}$	Cross-sectional average gas holdup	-
α	Proportional constant	-
ε_e	Gas holdup inside the envelop	-

η	Ratio of r/R	-
ρ	Phase density	Kg/m^3
Ψ	Stream function	-
σ	Surface tension	N/m
μ	Molecular viscosity	Pa.s
μ_T	Turbulent viscosity	Pa.s
μ_{eff}	Effective viscosity	Pa.s

Subscripts

ax	Axial coordinate
d	Downcomer
G	Gas phase
L	Liquid phase
max	Maximum value
r	Riser

Abbreviations

$2D$	Two-dimensional
$3D$	Three-dimensional
CFD	Computational Fluid Dynamics
EDM	Electro Diffusion Measurement
LDA	Laser Doppler Anemometry
LDV	Laser Doppler Velocimetry
PIV	Particle Image Velocimetry

List of Tables

Table	Title	Page
(3.1)	Interrelationship between the riser and the downcomer gas holdups in airlift reactors:	29
(4.1)	Local and average gas holdup and liquid velocity in riser and downcomer at 0.018634 m/s superficial gas velocity	40
(4.2)	Local and average gas holdup and liquid velocity in riser and downcomer at 0.040887m/s superficial gas velocity	41
(4.3)	Local and average gas holdup and liquid velocity in riser and downcomer at 0.056583 m/s superficial gas velocity	42
(4.4)	Local and average gas holdup and liquid velocity in riser and downcomer at 0.081263 m/s superficial gas velocity	43
(4.5)	Local and average gas holdup and liquid velocity in riser and downcomer at 0.094986 m/s superficial gas velocity	44
(4.5)	Local and average gas holdup and liquid velocity in riser and downcomer at 0.11419193 m/s superficial gas velocity	45

List of Figures

Table	Title	Page
(1.1)	Performance Targets for Computational Fluid Dynamics.	5
(2.1)	Three snapshots of the iso-surface of the bubble plume, the surface indicates ($\epsilon_G = 0.1$). The liquid velocity field in the centre plane is also shown. The plots are respectively 100, 200 and 300s after the start of the simulation.	12
(2.2)	Effect of liquid static height on transition velocity.	15
(2.3)	Effect of column diameter on transition velocity.	16
(3.1)	Flow regimes encountered in bubble columns (Urseanu and Krishna, 2000).	19
(3.2)	Flow regimes based on superficial velocity and column diameter (Urseanu and Krishna, 2000).	19
(3.3)	Schematic representation of equation (3.10).	32
(3.4)	Typical drift flux plot using Wallis (1969) approach (Deckwer <i>et al.</i> , 1981).	34
(4.1)	Schematic of airlift reactor, showing the computational domains and grid details.	38
(4.2)	Contours of air volume fraction and liquid velocity at 0.018634 m/s superficial gas velocity.	40
(4.3)	Contours of air volume fraction and liquid velocity at 0.040887m/s superficial gas velocity.	41
(4.4)	Contours of air volume fraction and liquid velocity at 0.056583 m/s superficial gas velocity.	42
(4.5)	Contours of air volume fraction and liquid velocity at 0.081263 m/s superficial gas velocity.	43
(4.6)	Contours of air volume fraction and liquid velocity at 0.094986 m/s superficial gas velocity.	44
(4.7)	Contours of air volume fraction and liquid velocity at 0.11419193 m/s superficial gas velocity.	45
(4.8a)	Comparison of airlift experimental data of Van Baten <i>et</i>	47

	<i>al.</i> (1999) with CFD simulations for average gas holdup in the riser.	
(4.8b)	Comparison of airlift experimental data of Van Baten <i>et al.</i> (1999) with CFD simulations for average liquid velocity in the riser.	47
(4.8c)	Comparison of airlift experimental data of Van Baten <i>et al.</i> (1999) with CFD simulations for average liquid velocity in the downcomer.	48
(4.9a)	Radial distribution of Gas holdup , for varying superficial gas velocity, at height 1.75m above the sparger.	50
(4.9b)	Radial distribution of liquid velocity in riser and downcomer, for varying superficial gas velocity, at height 1.75m above the sparger.	50
(4.10)	Effect of gas velocity on the axial liquid velocity at column center.	51
(4.11)	Identification of flow regime transition based on drift-flux method.	52
(4.12)	Effect of superficial gas velocity on the gas hold-up in riser of airlift reactor ($U_{G,trans} = 0.0899$ m/s).	53
(4.13a)	Comparison of gas holdup, for airlift reactor with bubble column of 0.15 m diameter.	54
(4.13b)	Comparison of centerline liquid velocity, $V_L(0)$, for airlift reactor with bubble column of 0.15 m diameter.	54
(4.14)	Identification of flow regime transition based on drift-flux method in bubble column of 0.15 m diameter.	55
(4.15)	Effect of superficial gas velocity on the gas hold-up in riser of bubble column of diameter 0.15 m ($U_{G,trans} = 0.04$ m/s).	56

CHAPTER ONE

INTRODUCTION

1.1 Bubble Columns

Bubble columns or airlifts are widely used in the chemical and biochemical process industry, conducting gas–liquid reactions in a variety of practical applications in industry such as absorption, fermentations, coal liquefaction and wastewater treatment. Due to their simple construction, low operating cost, high energy efficiency and good mass and heat transfer, bubble columns offer many advantages when used as gas–liquid contactors and develop design tools for engineering purposes [Deen, 2000; Mouza *et. al.*, 2004].

Bubble columns have been of particular interest recently due to the advantages over other reactor types. They are easy to use, affordable, and due to the low number of moving parts, they are easy to repair. Bubble columns provide excellent means for temperature control, effective mass transfer rates, and solid handling with little erosion or plugging problems [Martis, 2004].

Bubble columns are multiphase equipments used to bring into contact gas and liquid phases. Gas, that constitutes the dispersed phase, is distributed at the bottom of the column and rises as bubbles through the liquid that constitutes the continuous phase [Diaz *et. al.*, 2006]. Knowledge of liquid-phase mixing times, liquid circulation velocities and axial mixing (characterized by axial dispersion coefficients) is important for design and operation of bubble column and airlift reactors (Sa'nchez Miro'n *et. al.*, 1999, 2000).

Bubble column hydrodynamics is complex and characterized by different flow patterns depending on gas superficial velocity, liquid phase properties, sparger design, column diameter etc. Non uniform gas hold-up distribution within the vessel induces density fluctuations which originate circulation currents influencing strongly phase mixing and transfer parameters [Marchot *et. al.*, 2001].

Gas holdup and liquid circulation velocity are amongst the most widely studied parameters in airlift reactors. This emphasis attests to their significance. The difference in gas holdup between the riser and the down comer in an airlift reactor determines the magnitude of the induced liquid circulation velocity which in turn influences the bubble rise velocity, and the gas holdup. The holdup and the liquid velocity together affect the mixing behavior, mass and heat transfer, the prevailing shear rate, and the ability of the reactor to suspended solids. Clearly, all aspects of performance of airlift systems are influenced by gas holdup and liquid circulation [Chisti *et. al.*, 1998].

1.2 Computational Fluid Dynamics (CFD)

The numeric simulation in Fluid Mechanics and Heat and Mass Transfer, commonly known as CFD “Computational Fluid Dynamics”, has an expressive development in the last 20 years as a tool for physical problem analyses in scientific investigations, and nowadays as a powerful tool in solving important problems applied to engineering CFD permits a detailed investigation of local effects of different types of equipment, such as chemical and electrochemical reactors, heat exchangers, mixing tanks, cyclones, combustion systems, among others [Silva *et. al.*, 2005].

CFD can be regarded as an effective tool to clarify the importance of physical effects (e.g. gravity, surface tension) on flow by adding or removing them at will. An increasing number of papers deals with CFD application to bubble columns [Wild *et. al.*, 2003; Joshi, 2002]. Wild *et. al.*, (2003) cite the most important reasons for this increasing interest:

1. Measuring techniques applied to the local hydrodynamics in bubble columns made huge progresses so that more reliable local measurements are now available to check the adequacy of CFD predictions.
2. Increased computer capacity.
3. The quality of the different CFD program systems has been improved: better numerical methods, more realistic closure laws.
4. The occurrence of flow regimes, of deformable gas-liquid interfaces and the lack of knowledge about the closure terms (turbulence, bubble-bubble interactions) have transformed bubble column studies into a benchmark of all gas-liquid dispersed flows.

For the numerical computation of two-phase flows two approaches are mainly applied, namely the Euler/Euler and the Euler/Lagrange approach. The first method considers both phases as interacting continua, while in the second method the discrete nature of the dispersed phase is taken into account by tracking a large number of individual bubbles through the flow field [Lain *et. al.*, 2000].

1.2.2 Performance of CFD

By predicting a system's performance in various areas, CFD can potentially be used to improve the efficiency of existing operating systems as well as the design of new systems. It can help to shorten product and process development cycles, optimize processes to improve energy efficiency and environmental performance, and solve problems as they arise in plant operations. Also advances in CFD possible for the chemical and other low-temperature process industries. With these broad goals as a base, specific performance targets (both quantitative and qualitative) have been identified for CFD, as shown in fig. (1.1). These targets illustrate how improvements in computational fluid dynamics can have a wide- reaching impact throughout the entire chemical industry.

The impact of CFD on the process and product development cycle is greatest in the earliest phases (i.e., experimental optimization and scale-up). CFD facilitates the design process by increasing the reliability of the design, reducing or eliminating design errors, and allowing developers to visualize the results of a process design or innovation. It promotes innovation by making the design process shorter, less risky, and easier to accomplish. Using CFD to resolve problems with existing processes can reduce equipment failures and minimize poor operational performance, decreasing process shut-down time. When used to optimize plant and equipment operation, CFD can increase yields, providing a mechanism for incremental expansion.

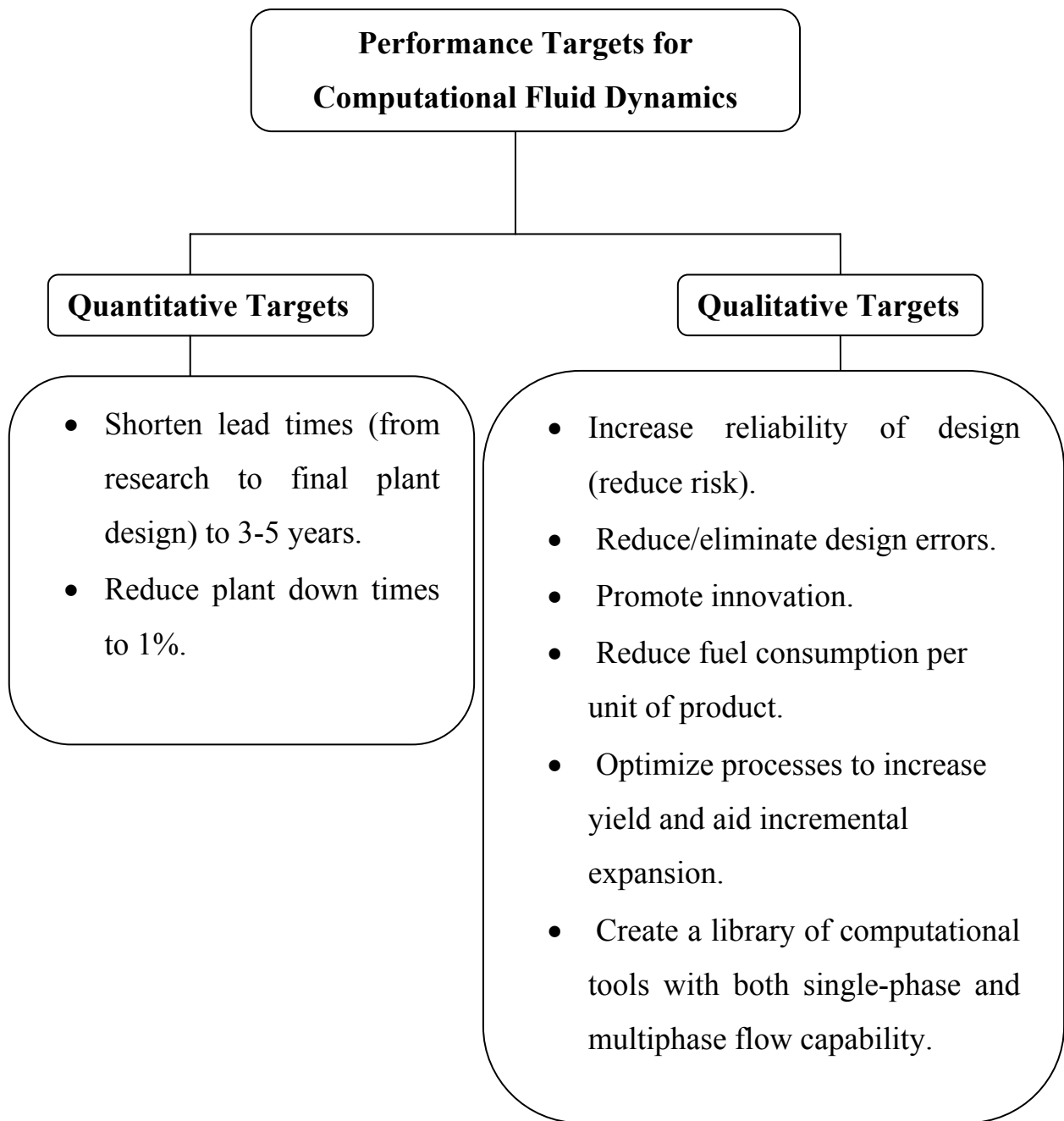


Figure (1.1) Performance Targets for Computational Fluid Dynamics (11)

1.2.3 Flow and Mixing Applications of CFD

1. Application model development.
2. Process and equipment optimizations, e.g. process yield, crystallizes, reactors.
3. Reactor design (STR, bubble column, static and rotor-stator mixers).
4. Process and reactor scale up.
5. Parameter sensitivity studies.
6. Temperature control strategies.
7. Monomer/initiator dosing strategies.
8. Equipment rating.
9. Troubleshoot existing design problems.
10. Evaluate retrofit options.[49]

1.2.4 Parameters of CFD

1. Velocity and turbulence fields.
2. Concentrations of reactants, products and by-products.
3. Product distribution.
4. Temperature profiles.
5. Gas hold up.
6. Particle size/chain length distributions.
7. Solids distributions.
8. Batch time.
9. Residence time distribution.
10. Power draw Mix times.
11. Heat transfer coefficient [49].

1.3 Aim of the Work:

This work is contributed in computational modeling studies of multiphase flows in process and oil industry. It is a necessary start with utmost attention being paid to numerical and physical fundamentals, which can be easily extended to analyze other multiphase flow reactors, like fluidized bed and bubble or slurry bubble columns. The main objectives of this work are:

Using computational fluid dynamic (CFD) as a tool to:

1. Measuring of some the hydrodynamics of airlift reactor, and comparing the results with experimental data.
2. Measuring transition liquid velocity and gas holdup in airlift reactor.
3. Comparing the hydrodynamic of airlift reactor with bubble column.
4. Measuring transition regimes for bubble column.

CHAPTER TWO

LITERATURE SURVEY

2.1 Gas Holdup

Gas holdup and liquid circulation velocity are amongst the most widely studied parameters in airlift reactors and bubble column. It can be defined as the percentage by volume of the gas in the two or three phase in the column.

Vatai and Tekic (1989) investigated the effect of the column diameter on the gas-holdup in bubble columns with pseudo plastic liquids. The influence of the superficial gas velocity, physical properties of liquids and column diameter (0.05, 0.1 and 0.2m) on the gas-holdup. They found that in the investigated range of the superficial gas velocity the column diameter has no influence on the gas-holdup in air-water system, and for high liquid viscosity the column diameter effected a change in the gas-holdup. In a small-diameter column large bubbles are stabilized by the column wall, which leads to transition to slug flow regime and an increase in the gas-holdup.

Shun and Yasuhiro (1990) investigates experimentally by using impulse response method, gas phase dispersion in bubble columns of 0.5 and 0.2m diameter at superficial gas velocities in the range 0.029-0.456 m/s. Based on the recirculation theory of bubble columns, expression for the axial dispersion coefficient of the gas phase was found:

$$\varepsilon_G = (180/\alpha) U_G D_T^{3/2} \quad \dots (2.1)$$

where this equation quantatively describe the experimental results with the proportional constant $\alpha = 9$. At gas velocity higher than 0.1m/s, the gas phase

dispersion was suppressed by the insertion of perforated plate with a free of 44%.

Nenes *et. al.* (1994) presented analysis of real field data collected from experiments on the outflow rate of the airlift pump, and a differential, two-phase hydrodynamic model for the simulation of airlift pumps. Predictions were obtained both by the hydrodynamic model and a mean air-volume fraction model, and compared with real field experimental data. Both models predicted correctly the overall behavioral trend of the experiments. However, they were shown that the predictions based on the hydrodynamic model were, in all cases, significantly better in comparison to the mean void fraction model. This is because the hydrodynamic model takes into account the gas compressibility itself (in the momentum and continuity equations) and all the effects that result from this (i.e., multiple flow regimes). The mean air-volume fraction model might give better predictions if a single flow regime were predominant along the up riser. However, for water wells of moderate to large depths, the compressibility effects of the gas phase are large, which among other things leads to multiple flow regimes.

Ursula, Hans (2004) performs tracer experiments (jump responses) both experimentally and also numerically. In both cases resulting data is then analyzed with the aid of the convection-dispersion models that the integral quantities gas hold-up, axial dispersion coefficient and mean residence time show sufficient sensitivity with respect to the accuracy with which the physical properties of the bubble column and the fluid flow are captured by the computational grid, the boundary conditions and the sub-models for interfacial momentum exchange.

Delmas *et. al.* (2006) performed investigation of local hydrodynamics in a pilot plant bubble column using various techniques, exploring both axial and radial variations of the gas hold-up, bubble average diameter and

frequency, surface area. Explored up a wide range of operating conditions to large gas and liquid flow rates, with two sparger types. They found that very strong effect of liquid flow on bubble column hydrodynamics at low gas flow rate. First the flow regime map observed in batch mode is dramatically modified with a drastic reduction of the homogeneous regime region, up to a complete heterogeneous regime in the working conditions ($U_G > 0.02$ m/s). On the contrary, liquid flow has limited effects at very high gas flow rates.

2.2 Axial Liquid Velocities

Viswanathan *et. al.*, (1983) developed the mathematical model based on the force balance to estimate circulation in cylindrical columns. The model gave axial and radial variation of axial liquid velocity as a function of flow strength. Flow strength equation is:

$$F_s = d_l L_l^2 u_{br} \left[\frac{g L_l^3 U_G}{b_3 R^2 u_{br}^3} \right]^{1/d_2} \quad \dots (2.2)$$

The axial and radial variation of axial liquid velocity is:

$$u_z \Big|_{z=0} = \frac{I}{(1 - \varepsilon_e) r} \frac{\partial \psi}{\partial r} \Big|_{r=0} = \frac{2 A \pi^2}{L_l^2 (1 - \varepsilon_e)} \sin \left(\frac{\pi z}{L_l} \right) \quad \dots (2.3)$$

and

$$u_{z-avg} = \frac{1.2 A}{R^2} [1 + 0.6 \eta^2 - 3.32 \eta^4 - 0.92 \eta^6] \quad \dots (2.4)$$

The analytical expressions derived analytical expressions for estimating the flow strength besides simplifying calculation provides.

2.3 Numerical Simulation in Fluid

Solbakken and Hjertager (1998) demonstrate CFD as a tool for scale up of bubble column an industrial full-scale fermentation bubble column.

Bohn (2000) used 3D simulation of bubble column; gas holdup was calculated by plotting the distribution of gas volume fraction vs. column height. The plot showed a point where the concentration of gas increased rapidly which is the gas-liquid interface. The next step was to compare the height of liquid gas interface to the original height of liquid height interface. The expansion, or amount of liquid gas interface rose, showed how much gas holdup in the reactor, from which the gas holdup is easily calculated.

Michele (2001) presented the Electro Diffusion Measurement technique (EDM) and computational results inside the 0.63 m diameter, 6 m high bubble column and show that only a reasonable combination of these two approaches can deliver new insights into physical phenomena and finally yield tools helpful in reactor design and scale-up. Measurement results of local dispersed phase holdups and liquid velocities delivered a strong foundation for CFD model development and verification documenting possibilities and limitations of implemented modeling strategies.

Deen *et. al.* (2000) used the commercial code CFX 4.3 to simulate the gas-liquid flow in 3D rectangular bubble columns. The movement of a bubble plume in a 3D bubble column was also simulated fig. (2.1). In contrary to the other case only little temporal behavior was found. This disagrees with the strongly time dependent flow, which was observed experimentally. In the simulation the bubble plume moves into one corner and stays there for the rest of the simulation time. This resulted in asymmetric velocity profiles. The velocity profiles are better predicted higher up in the column.

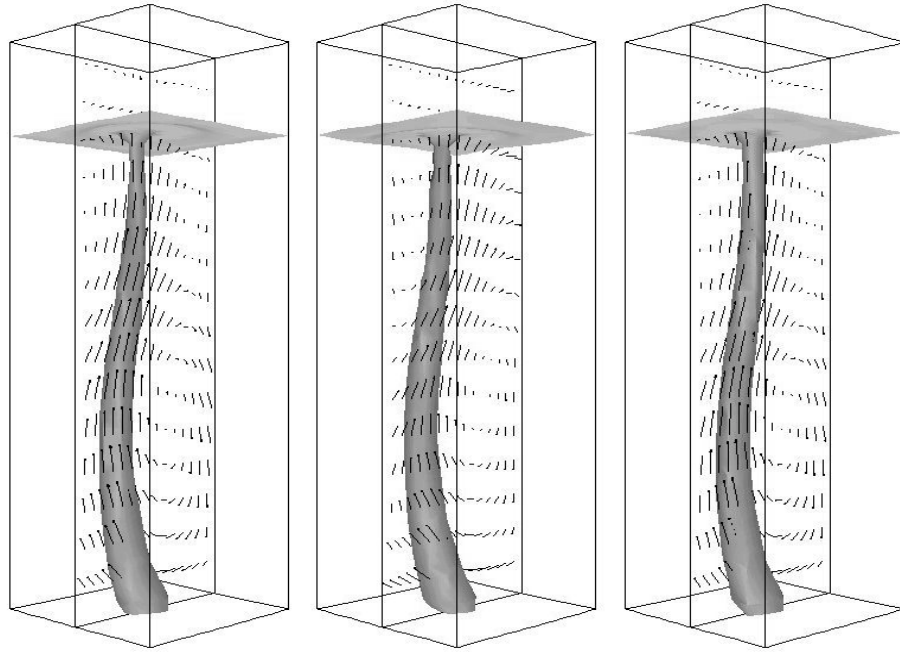


Figure (2.1) three snapshots of the iso-surface of the bubble plume, the surface indicates ($\epsilon_G = 0.1$). The liquid velocity field in the centre plane is also shown. The plots are respectively 100, 200 and 300 s after the start of the simulation [Deen *et. al.*,2000].

Buwa and Ranade (2003) focused on predicting time average flow properties with the help of few adjustable parameters. While times averaged characteristics can help provide general guidelines for reactor design, the effects of the unsteady flow characteristic are lost. CFD simulations of the bubble column have been performed using several multiphase approaches, which performed to study the effects of superficial gas velocity, sparger configuration (including bubble diameter), and the height to width (H/W) ratio of the column on the low frequency oscillations and time averaged flow variables ,such as vertical liquid velocity and gas holdup . The result indicated that the dynamic characteristics are sensitive to bubble size, as produced by different sparger configurations.

Klein *et. al.* (2003) showed how the design of enlarged separator by simple alteration of the diameter (A_D / A_R) and height (H_{DT} / H_C) of the draft tube in the internal-loop airlift reactor could effectively affect the

hydrodynamics of three-phase flow in the airlift reactor. The results showed similar solids distribution in the riser and down comer; however, uniform distribution was achieved only at higher gas flow rates. A very low solids holdup in the enlarged separator zone was found, this parameter showing a low sensitivity to changes of the air flow rate. The observations lead to the conclusion that an airlift reactor with dual separator and an A_D/A_R ratio around 1.2-2.0 can be suitable for batch/continuous high cell density systems, where uniform solids distribution, an efficient separation of particles from the liquid phase (upper part of the separator zone), and the maintenance of the bubbles inside the reactor (narrow part) is desirable. In addition, the lower part of the dual separator acts as an efficient mixer, which can significantly help to improve the overall mixing in the airlift reactor. A three-phase fluid model was used to predict the hydrodynamic parameters liquid velocity, gas holdup and solids distribution data. It was shown that the model could satisfactorily describe the behavior of a three-phase airlift reactor with a significantly enlarged head zone, if the solids distribution between the separator and the riser/down comer zones is known. The results of this study coupled with the model predictions may be applied to suggest optimal design (in terms of hydrodynamic behavior) of a batch/continuous three-phase airlift reactor for high cell density fermentations.

Gobby and Hamill (2003) demonstrated the progress that has been made in the modeling of complex multi-phase flows. In particular, the use of coupled solvers for the Multi-Phase flows, together with features such as the Population Balance Models and Generalized Grid Interfaces, is enabling the incorporation of more realistic physical models, much more quickly than in previous generations of CFD software.

Vladimir and Andrei (2003) presents the results of computational fluid dynamics (CFD) modeling of gas liquid flows in water electrolysis systems.

CFD is used as a cost-effective design tool to optimize the performance of different water electrolysis units. CFD software is used as a framework for analyzing the gas-liquid flow characteristics (pressure, gas and liquid velocities, gas and liquid volume fraction). The analysis is based on solving the couple two-fluid conservation equations under typical and alternative operating conditions with appropriate boundary conditions, turbulence models and constitutive inter-phase correlations. Numerical results have been validated based on the experimental available for a low-pressure data cell.

Mouza *et. al.* (2004) motivated by the need to develop reliable predictive tools for bubble column reactor design using a CFD code. Population balance equations combined with a three-dimensional model were used in order to study the operation of a rectangular bubble column. In addition, the mechanisms of bubble coalescence and break-up were considered into the Eulerian-Eulerian simulation, while being applied to a multiple size group model. Computational results have been compared to experimental data and it appears that bubble size distribution, axial liquid velocity and gas holdup can be well predicted at the homogeneous regime for the air-water system. The results acquired for the air-water system were encouraging and the simulations are to be extended to gas-liquid systems where the liquid phase is other than water. However, additional experimental work at the microscopic level combined with theoretical analysis are considered necessary for establishing CFD codes that will successfully predict the behavior of bubble column reactors.

Blazej *et. al.* (2004) used the simulation of two-phase flow for an experimental airlift reactor data and compared with the experimental data obtained by the Tracking of a magnetic particle and analysis of the pressure drop to determine the gas hold-up. Comparisons between vertical velocity and

gas hold-up were made for a series of experiments where the superficial gas velocity in the riser was adjusted between 0.01 and 0.075 m/s.

2.4 Transition Regime

Predictions of flow regime transition have been achieved by the development of various models and approaches that include pure empirical correlations, semi empirical and phenomenological models, linear stability theory, and Computational Fluid Dynamics (CFD).

Sarrafi *et al.* (1999) found that an increase in liquid static height decreases transition velocity up to 4 m as shown in figure (2.2). Beyond this, it almost becomes independent of liquid height. The ranges of column diameters, sparger hole diameters, and perforation pitches for these data were 0.14-0.16 m, 0.001-0.002 m, and 0.02 m, respectively.

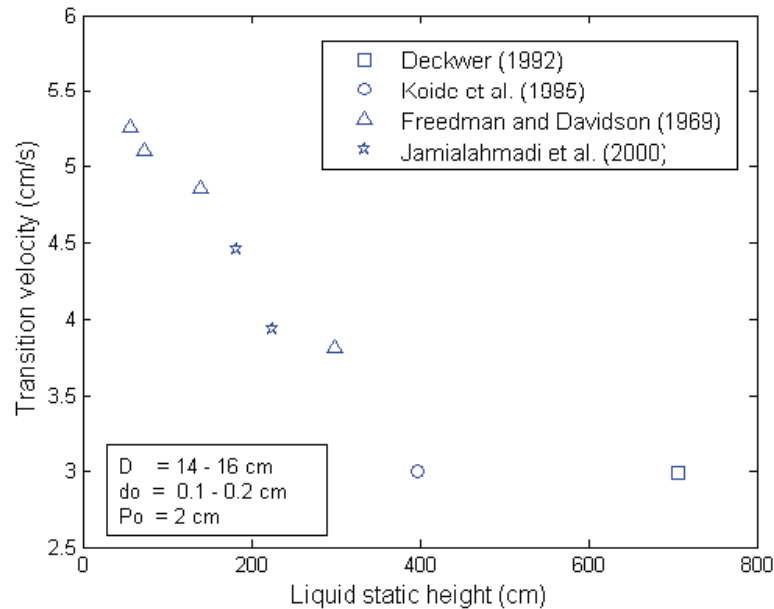


Figure (2.2) Effect of liquid static height on transition velocity, [Sarrafi *et al.* ,1999].

Ruzicka *et. al.* (2001) utilized the gas holdup data from three different column diameters (0.14, 0.29, and 0.4 m) to calculate transition velocity. At different liquid static heights they found that an increase in column diameter reduced transition velocity as shown in figure (2.3).

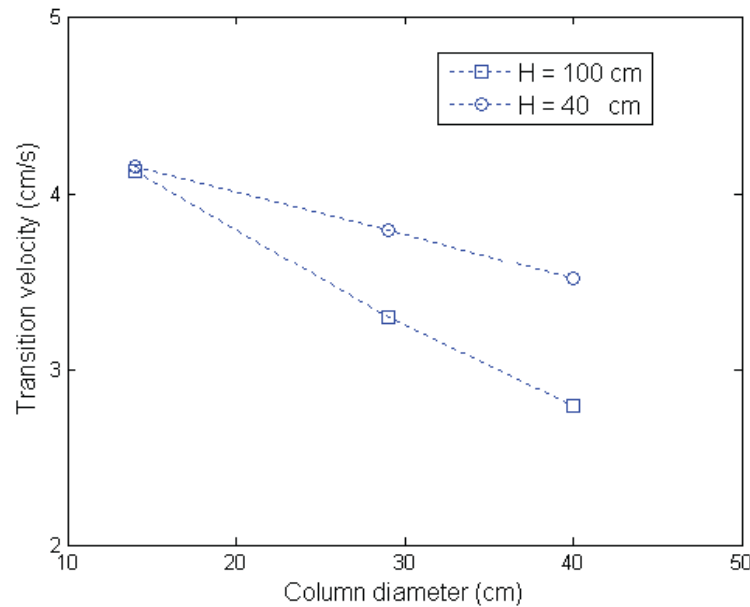


Figure (2.3) Effect of column diameter on transition velocity, [Ruzicka *et. al.*, 2001].

Martis (2004) used bubble column of a 4-inch diameter plexus-glass cylinder. Gas holdup and flow regime transition velocity measurements in a bubble column reactor were made. A transition velocity between homogeneous and heterogeneous of about 3cm/s was found. The transition velocity was found to be unaffected by standing water column height, provided that the height was larger than the diameter of the column.

Zhe Cui (2005) investigates the hydrodynamics in a high pressure bubble column is experimentally, measure the liquid vertical and horizontal velocities using an LDV (Laser Doppler velocimetry) technique, obtains The Reynolds shear and normal stresses, discusses the effect of the pressure on the transition of the flow regime, flow field and the Reynolds stresses, and

investigates Furthermore, the effects of the liquid properties on the hydrodynamics of the bubble column.

Diaz *et. al.* (2006) used a partially aerated plate and the combined effect of U_G and the liquid height/width of the column ratio (aspect ratio (H/W)) on the resulting flow regimes is studied. The use of partially aerated plates can generate bubble plumes that show an oscillatory movement and create ascending and descending liquid circulation structure. The resulting unsteady flow patterns differ considerably from the time-averaged flow regimes. The quantitative analysis of the flow regimes is based on the measurements of wall pressure fluctuations while qualitative description of the type of flow is obtained by image analysis. The analysis of existing time-averaged flow patterns for given experimental conditions is based on the representation of the global gas hold-up (ε_G) versus U while the study of non-stationary structures is based on the spectral analysis, a method that provides information of the oscillation frequency of the bubble plume as well as of the different physical phenomena taking place in the bubble column through the resulting spectra and the mean and characteristic frequencies.

CHAPTER THREE

THEORITICAL ASPECT

3.1 Hydrodynamic in Bubble Column and Airlift Reactor

The hydrodynamics of airlift reactor is strongly affected by liquid properties as well as by reactor design and operating conditions. A variety of hydrodynamic regimes establish in the airlift, depending on the choice of design parameters and tuning of operating conditions [Olivieri *et al.*, 2006].

Gas is dispersed into bubbles using a sparger and bubbles rise through the liquid. Hence, momentum is transferred from the faster, upward moving gas phase to the slower liquid phase. Depending on the gas and liquid flow rates and the physical properties of the system, bubble columns can be operated in either homogeneous bubbling flow, heterogeneous bubbling flow or slugging flow regimes. Bubbles play an important role in gas-liquid system. [Zhe Cui, 2005].

3.2 Factors Influencing Hydrodynamics of Bubble Column Reactors

Factors that influence hydrodynamics of Bubble Column Reactors are superficial velocity, bubble diameter, column geometry (reactor walls) and pressure [Urseanu and Krishna, 2000].

These factors are interdependent requiring them to be discussed in relation to each other rather than independently. Superficial gas velocity can be defined as volumetric gas flow rate per cross sectional area of bubble column. Superficial velocity is dependent on column dimensions [Miron *et al.*, 1999]. Figure (3.1) shows that an increase in superficial gas velocity will

cause bubble flow to change from a homogeneous flow regime to a heterogeneous flow regime.

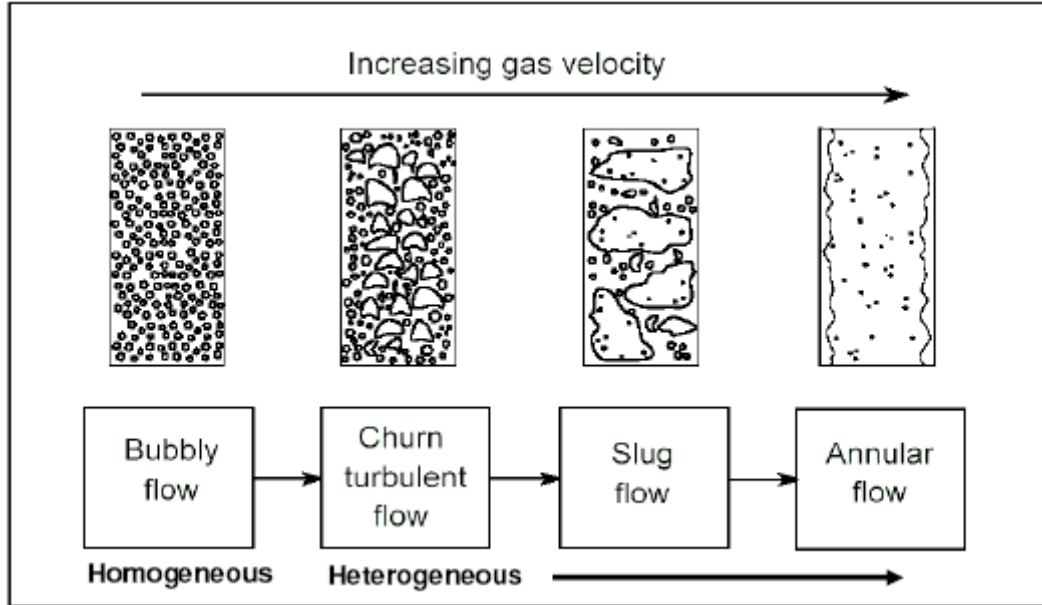


Figure (3.1) Flow regimes encountered in bubble columns (Urseanu and Krishna, 2000).

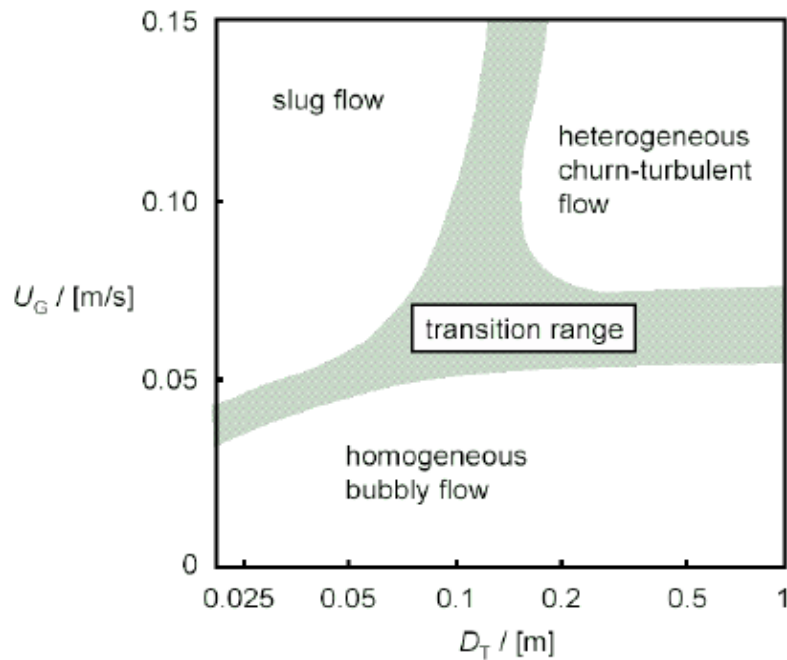


Figure (3.2) Flow regimes based on superficial velocity and column diameter (Urseanu and Krishna, 2000).

Figure (3.2) shows that the approximate transition from homogeneous bubble flow to heterogeneous churn-turbulent flow and slug flow is based on the superficial gas velocity and column diameter [Urseanu and Krishna, 2000]. For a given bubble column, the superficial gas velocity at which transition occurs would be different for sparged systems because sparged systems have a fixed number of openings and fixed opening size [Anderson, 2004].

The amount of time the bubble spends in the column is also dependent up on the height of the bubble column. In a taller bubble column the bubble has to travel a greater distance allowing more time for mass transfer. Generally taller bubble columns are preferred over shorter columns to improve mass transfer efficiency [Anderson, 2004].

Wall effects were found to be negligible in a bubble column with a single opening and a ratio of bubble diameter to column diameter less than 0.125 [Krishna *et. al.*, 1999].

Bubble diameter and gas holdup can be related by equation (3.1) (Poulsen and Iversen, 1998; Miron *et. al.*, 2000]. The larger the bubble diameter, the larger the interfacial surface area is which leads to more mass transfer due to large gas holdup. A large number of dense small bubbles are preferred over a small number of large bubbles. The effective interfacial area of a swarm of small bubbles is greater than for a few large bubbles.

$$a_L = \frac{6 \varepsilon}{d_b (1 - \varepsilon)} \quad \dots (3.1)$$

Pressure affects the flow of bubbles in bubble columns. When external pressure is applied on the bubble column, bubbles are more homogenous and the mean bubble velocity is small, increasing gas holdup, and increasing mass transfer [Anderson, 2004].

The pressure effect on the flow regime transition is mainly due to the change in bubble characteristics, such as bubble size and bubble size distribution. When bubble column operate at high pressure condition, bubble coalescence is suppressed and bubble breakup is enhanced. Also, the distributor tends to generate smaller bubbles. All these factors contribute to small bubble sizes and narrow bubble size distributions and, consequently, delay the flow regime transition at high pressures. [Zhe Cui, 2005].

By comparing the pressure effect on the gas holdup with that on the bubble rise velocity, it can be stated that the increase in gas holdup with pressure is a consequence of the decreases in both the bubble size and the bubble rise velocity, i.e. larger bubbles broken into smaller ones and their rise velocities further reduced by pressure. The decrease in bubble rise velocity occurs due to corresponding variations of gas and liquid properties with pressure [Fan *et. al.*, 1998].

Buoyancy force of a bubble is a function of cube of bubble diameter and drag force is a function of square of bubble diameter (Adkins *et. al.*, 1996). As the bubble rise from the bottom of the reactor bubble diameter increases. With the change in diameter of the bubble the buoyancy force and drag force change, and in turn change the velocity of the bubble. The mean bubble velocity changes from inception to death or burst at the top of the column [Anderson, 2004].

3.3 Flow Regime

Bubble column flow regimes are broadly classified as homogeneous and heterogeneous flows (Krishna and Baten, 2003).

3.3.1 Homogenous Flow

The homogeneous regime is encountered at relatively low gas velocities and characterized by "small" bubbles, typically in the range of 2 to 6 mm, a narrow bubble size distribution and The rise velocity of these bubbles does not exceed 0.025 m/s and radially uniform gas holdup and is most desirable for practical applications, because it offers a large contact area [Joshi *et. al.*, 2002; Olmos *et. al.*, 2001].

The concentration of bubbles is uniform, particularly in the transverse direction. The process of coalescence and dispersion are practically absent in the homogeneous regime and hence the size of bubbles are entirely dictated by the sparger design and the physical properties of the gas and liquid phases [Tharat, 1998].

Observed change from bubbly flow to transition flow is asymptotic depending on various factors [Wallis, 1969] which affect the size of the gas bubble by altering the degree of coalescence. The flow regime transition is normally identified based on instability theory, analysis of fluctuation signals, and the drift flux model. Higher gas density is found to have a stabilizing effect on the flow and that the gas fraction at the instability point (i.e., transition point) increases with gas density, while the gas velocity at the instability point only slightly increases with gas density. The drift flux of gas increases with the gas holdup in the dispersed regime; in the coalesced bubble regime, the rate of increase is much larger [Zhe Cui, 2005].

3.3.2 Heterogeneous Flow

Heterogeneous flow is characterized by larger bubbles formed when small bubbles coalesce and interact with each other and, as a result, the bubbles have a range of speeds in varied directions. The non-uniform gas

holdup distribution across the radial direction causes bulk liquid circulation in this flow regime [Shaikh and Al-Dahhan, 2007]. Heterogeneous bubble flows are further classified into churn turbulent flow; slug flow and annular flow as shown in figure (3.1) [Urseanu and Krishna, 2000].

3.3.2.1 Churn-Turbulent Flows

Phenomenologically churn-turbulent flows can be readily described as follows. At high superficial gas velocities and low liquid superficial velocities in large diameter vessels high gas holdups are reached (typically well in excess of 30%) and large spiraling, transient, vortex like structures move through the column [Hills, 1975, Devanathan, 1991, Chen *et al.*, 1994].

3.3.2.2 Slug Flow

This flow is characterized by long “Taylor” bubbles rising and almost filling a pipe’s cross-section. Liquid moves around the bubbles and fills the space between two successive gas slugs. While the progress of the gas slugs is very stable, the area between it is greatly agitated. In industry, slug flow may appear in nearly any application employing two-phase flow in pipes [Von Karman, 2006]. This type of flow is characterized by large regions of a lower density fluid (bubble) surrounded by regions of a higher density fluid (slugs). From fig. (3.2), it can be inferred that the mean bubble velocity in slug flow would be high (>0.05 m/s) [Urseanu and Krishna, 2000]. Slug flow regime transition occurs at constant overall gas holdup [Shaikh and Al-Dahhan, 2007].

3.4 Bubble Formation

The size of bubbles generated from gas distributors have a significant effect on the hydrodynamics and mass transfer in bubbling systems. An increase in gas density was found to reduce the size of bubbles. Discrete bubbles are formed at low gas velocities. At a high gas velocity, jetting occurs and bubbles are formed from the top of the jet. In the discrete bubble regime, the bubble size is relatively uniform; in contrast, the bubbles formed from a jet are of a wide size distribution [Massimilla *et. al.*, 1961]. The empirical correlation provided by Idogawa *et. al.* (1987) indicated that the bubbling-jetting transition velocity in a liquid is proportional to the gas density to the power of -0.8. Increasing the air flow increases the frequency of bubble formation, and, consequently [Nguyena *et. al.*, 1996].

The stability at larger gas fractions is only possible when the bubble size is small. Larger bubbles cause large-scale turbulence, also at lower gas fractions. The bubbles experience a horizontal lift force. Its direction depends on the bubbles' size and shape – larger bubbles are flatter. Larger bubbles tend to be drawn to the centre of the column, where they cluster, cause a lower fluid density, and cause large vortices. The larger bubbles, the sooner a flow becomes turbulent. It is therefore necessary to integrate the effect of the lift force into the computer models [Wouter, 2006].

3.5 Bubble Coalescence and Break-up

The coalescence of two bubbles is often assumed to occur in three steps. First the bubbles collide trapping a small amount of liquid between them. This liquid film then drains until the liquid film separating the bubbles reaches a critical thickness. The film ruptures and the bubbles join together. The coalescence process is therefore modeled by a collision rate of two

bubbles and a collision efficiency relating to the time requires for coalescence (t_{ij}) and the contact time (τ_{ij}). Prince and Blanch (1990) considered the collisions resulting from three different mechanisms, turbulence (θ_{ij}^T), buoyancy (θ_{ij}^B) and laminar shear (θ_{ij}^{LS}). The total coalescence rate is:

$$Q_{ij} = (\theta_{ij}^T + \theta_{ij}^B + \theta_{ij}^{LS}) e^{(-t_{ij} / \tau_{ij})} \quad \dots (3.2)$$

The birth rate of group-i bubbles due to coalescence of group-j and group-k bubbles is:

$$B_C = \frac{I}{2} \sum_{j=1}^i \sum_{k=1}^i Q_{jk} n_j n_k \quad \dots (3.3)$$

The death rate of group-i bubbles due to coalescence with other bubbles is:

$$D_C = n_i \sum_{j=1}^N Q_{ij} n_j \quad \dots (3.4)$$

[Prince and Blanch, 1990].

A simple model for break-up, first presented by Geary and Rice (1991b), is employed. The basis of a bubbles break-up mechanism is related to the turbulent kinetic energy and its dissipation:

$$d_s = C_{SMD} \cdot \frac{k^{3/2}}{\varepsilon} \quad \dots (3.5)$$

C_{SMD} is a tuning parameter and is given the value 0.04.

CFD calculations of dispersed two-phase flows, the particles are assumed to have the same size and shape, i.e. the mono-disperse assumption. In reality a wide spectrum of particle sizes and shapes exist at every point. Particularly, in gas-liquid flows it is almost impossible to control the sizes and shapes of the bubbles and droplets when break-up and coalescence occur [Simon Lo, 2000].

3.6 Bubbles Motion

In airlift reactors larger bubbles rise with liquid in the riser section. On the other hand, smaller bubbles are carried downward by liquid circulation in both the riser and down-comer sections. However, the actual amount of air that circulates through the down-comer is quite small [Kumar, 2006].

As the characteristics of bubble motion and bubble interfacial dynamics govern the performance of the bubbling systems, the understanding and hence the ability of controlling the bubble motion and interfacial dynamics are important to effective operation of these systems.

However, in the reality, rising bubbles with a diameter larger than 5 mm are always not spherical. Bubbles oscillate with a certain frequency during the rising period [Zhe Cui, 2005].

In the churn turbulent regime the "large" bubbles ($d_B > 0.015$ m) formed by coalescence of small bubbles are rising much faster, typically in the range of 1-2 m/s. They "churn" up the liquid phase and cause an intense mixing in the column. As an opposite phenomenon to the coalescence, the large bubbles are breaking up. Therefore the "dynamics" of large bubbles is continuously determined by bubble-bubble interaction, characterized by high frequency coalescence and breaking up.

3.7 Relationship between the riser and down comer gas holdup in airlift reactors:-

The volumetric flow rate of liquid in the riser of an airlift reactor can be expressed in terms of the superficial liquid velocity in the riser and its cross sectional area; thus,

$$Q_{Lr} = U_{Lr} A_r \quad \dots (3.6)$$

where Q_{Lr} is the liquid flow rate, U_{Lr} is the superficial liquid velocity in the riser, and A_r is the riser cross-sectional area. Similarly, for the down comer we have

$$Q_{Ld} = U_{Ld}A_d \quad \dots (3.7)$$

where U_{Ld} is the superficial liquid velocity in the down comer and A_d is the down comer cross-sectional area. Because all the liquid exiting the down comer circulates through the riser, i.e., $Q_{Lr} = Q_{Ld}$, from eqs (3.6) and (3.7), we have

$$U_{Lr}A_r = U_{Ld}A_d \quad \dots (3.8)$$

Equation (3.8) can be written in terms of the linear liquid velocities in the various zones:

$$V_{Lr}A_r(1 - \varepsilon_r) = V_{Ld}A_d(1 - \varepsilon_d) \quad \dots (3.9)$$

Where V_{Lr} and V_{Ld} are the linear liquid velocities in the riser and down comer, respectively, and ε_r and ε_d are the respective gas-holdups.

Rearrange of equation (3.9) leads to

$$\varepsilon_d = \frac{V_{Lr}A_r}{V_{Ld}A_d} \varepsilon_r - \left(\frac{V_{Lr}A_r}{V_{Ld}A_d} - 1 \right) \quad \dots (3.10)$$

Equation (3.10) is an explicit relationship between the riser and down comer holdups. The equation is quite general and it applies to any airlift reactor, irrespective of the liquid and the gas phases used. Equation (3.10) may be written as

$$\varepsilon_d = \alpha \varepsilon_r - \beta \quad \dots (3.11)$$

where

$$\alpha = \frac{V_{Lr} A_r}{V_{Ld} A_d} \quad \dots (3.12)$$

and

$$\beta = \alpha - 1 \quad \dots (3.13)$$

Equation (3.11) has the same form as many empirical correlations found in table (3.1). Frequently, β has been neglected as being negligibly small, and equ. (3.11) has been simplified to

$$\varepsilon_d = \alpha \varepsilon_r \quad \dots (3.14)$$

A multitude of correlations such as equations (3.11) and (3.14) are available as summarized in table (3.1); however, most of those equations differ on the values of the parameters α and β .

The parameters α and β supposedly depend on the geometry of the reactor (internal or external loop), the liquid and gas phases used, and the regime of the operation. The α -values have normally ranged over 0.8-0.9 (Chisti, 1989). Lower value of α have been reported, but values equaling unity or higher have never been observed.

Note that a constant value of α in a given reactor implies that the ratio V_{Lr}/V_{Ld} is not sensitive to the gas flow rate or the gas holdup in the riser. This appears to be the case over much of the operational range for internal loop type of airlift reactors without especial gas-liquid separators. However, a constant V_{Lr}/V_{Ld} can not be assumed generally; hence, in some cases the linear equation (3.11) could break down. This would happen mostly in airlift devices with gas-liquid separators. With an effective gas-liquid separator, the down comer gas holdup will be nil, and equation (3.11) will be take the form

$$\varepsilon_r = 1 - \frac{1}{\alpha} \quad \dots (3.15)$$

Because the riser gas holdup must increase with increasing gas flow rate, the α -value must increase. In a reactor with no gas in the down comer, the bounds of variation of α can be shown to be $0 \leq 1/\alpha \leq 1$.

Table (3.1) Interrelationship between the riser and the down comer gas holdups in airlift reactor [Chisti, *et. al.*, 1998]:

Reactor	Equation	System and Geometry	Reference
1. Annulus sparged concentric draft-tube reactors	$\varepsilon_d = 0.89 \varepsilon_r$	Air-water $A_d/A_r = 0.13, 0.35,$ or 0.56	Bello (1981)
2. Split-cylinder device	$\varepsilon_d = 0.997 \varepsilon_r$	Air-water and air-salt solution (0.15M sodium chloride) $A_d/A_r = 0.411$	Chisti (1989)
3. Draft-tube sparged internal-loop	$\varepsilon_d = (0.863 \pm 0.004) \varepsilon_r$	Air-salt solution (0.02M potassium chloride) $A_d/A_r = 0.78$	Bakker <i>et al.</i> (1993)
4. Multiple internal-loop airlift	$\varepsilon_d = (0.875 \pm 0.006) \varepsilon_r$	Air-salt solution (0.02M potassium chloride) $A_d/A_r = 0.31, 0.43, 0.91$	Bakker <i>et al.</i> (1993)
5. Draft-tube sparged internal-loop	$\varepsilon_d = 0.8 \varepsilon_r \left(1 + 20 d_p\right) \left(1 + \frac{W_s}{W_L}\right)^{-0.46}$	Suspensions of calcium alginate beads $\rho_s = 1030 \text{ kgm}^{-3};$ $d_p = 1\text{-}3.6 \text{ mm};$ loading = 0-30% vol.	Lu <i>et al.</i> (1995)

6. Split-cylinder internal loop	$\varepsilon_d = 0.63 \varepsilon_r - 0.0008$ $\varepsilon_d \geq 8 \times 10^{-4}$	Animal cell microcarriers in 0.1M aqueous sodium chloride $\rho_s=1030-1050$ kgm ⁻³ ; $d_p= 150-300$ μ m; 0-30 kgm ⁻³ solids loading; $A_r/A_d = 1$; $U_{Gr} = (0-6.7) \times 10^{-3}$ ms ⁻¹	Ganzeveld <i>et al.</i> (1995)
7. Draft-tube sparged internal-loop	$\varepsilon_d = C \varepsilon_r$ <p>C depended on sparger hole diameter $0.770 \leq c \leq 0.798$ for $30 \leq \delta (\mu\text{m}) \leq 1000$</p>	Sea water. Sintered glass and perforated pipe spargers $A_d/A_r = 1$	Contreras (1996)
8.Split cylinder internal-loop (liquid level below upper edge of baſe)	$\varepsilon_d = (0.889 + 2.972 h_c) \varepsilon_r - 0.642$ $h_c = \frac{h_b - h_L}{h_b}, \quad h_L < h_b$	Air-water $A_r/A_d = 2.44$ $h_c = 0.029-0.120$	Wenge <i>et al.</i> (1996)
9. External-loop reactors	$\varepsilon_d = 0.79 \varepsilon_r - 0.057$	Air-water and aqueous salt solutions $A_r/A_d = 2.273, 4.000, 9.091$	Bello (1981)
10. External-loop reactors	$\varepsilon_d = 0.4760 \varepsilon_r - 0.024$	Air-water, air-salt solution (0.15M sodium chloride), 1 and 2% (wt/vol) slurries of cellulose fibers in aqueous sodium chloride (0.15M) $A_d/A_r = 0.25, 0.44$	Chisti (1989)

When the V_{Lr}/V_{Ld} ratio varies little with gas flow rate, equation (3.10) may be approximated as the solid straight line shown in the figure (3.4). This line has negative y-intercept. Note that the y-intercept can never be a positive number because this would be implying a down comer gas holdup value that is higher than the riser holdup. Therefore the slope of the line, or the parameter α in equation (3.11), must always be greater than unity albeit slightly. This is inconsistent with all the empirically determined correlations table (3.1) because they all yield α -values that are below one. Normally, the y-intercept has a low absolute value (in the order of 10^{-3} – 10^{-4}). This means that α in equation (3.11) can be very close to 1; however α value should not be less than one. In fact, equation (3.14), with α equal to one (which is the only theoretically possible value in this equation), is the upper limit of equ. (3.10). The lines representing eqs. (3.14) and (3.10) will cross at the hypothetical extreme where $\varepsilon_r = \varepsilon_d = 1$ (A in fig. (3.4)). Therefore any linear correlation relating ε_d and ε_r must have a slope greater than unity and a y-intercept lower than zero.

At ε_r -value just greater than at point B in figure (3.4) the gas begins to recirculate in the down comer. At point B $\varepsilon_r = 0$, and from equation (3.10), the riser gas holdup is given by

$$\varepsilon_r = 1 - \frac{V_{Ld} A_d}{V_{Lr} A_r} \quad \dots (3.16)$$

Equation (3.16) provides the minimum value of the riser holdup that needs to be exceeded to obtain recirculation of gas into the down comer. That a minimum or ‘critical’ value of ε_r should exist is consistent with observation of [Ganzeveld *et al.*, 1995; wenge *et al.*, 1996]. With a higher value of riser holdup at point B, higher is the slope of the line and higher is the rate of increase of down comer holdup. As seen in equ. (3.16), the value of the riser

holdup needed to obtain recirculation of gas in the down comer depends on the liquid velocity in the down comer and the riser.

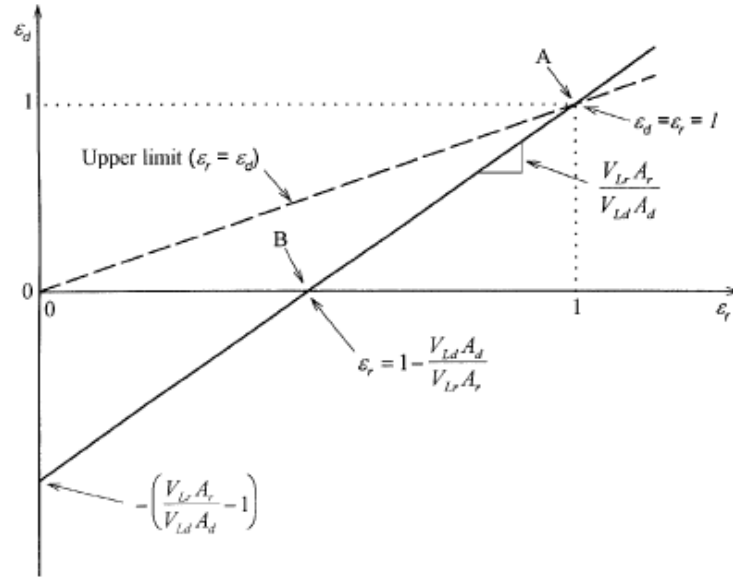


Figure (3.3) Schematic representation of equation (3.10).

3.8 Axial liquid velocity

The development of liquid velocity profiles along the axial direction is examined by the measurements of liquid velocity profiles at different axial positions above the distributor [Zhe Cui, 2005].

Average liquid velocity was related to superficial liquid velocity by [Taitel *et al.*, 1980]:

$$V_L = \frac{U_L}{1 - \varepsilon_G} \quad \dots (3.13)$$

Liquid circulation velocity distinguishes airlift from bubble column contactors where the average liquid velocity is zero. Liquid velocity in the airlift contactor was determined as a function of the superficial gas velocity, v_G , using the flow-follower method [Mercer, 1981].

Maximum centerline axial liquid velocity depending on reactor diameter, superficial gas velocity, liquid viscosity and density [Riquarts, 1981] and given as:

$$V_{l,ax,max} = 0.21 \cdot \sqrt{D \cdot g} \left(\frac{U_{G,0}^3 \cdot \rho_t}{\mu_l \cdot g} \right)^{1/8} \quad \dots (3.14)$$

Correlations for the prediction of radial profiles of axial liquid velocity have been presented by [Kawase and Moo-Young, 1986] have presented a rather simple correlation for radial profiles of axial liquid flow velocity in two-phase bubble columns:

$$\frac{V_L}{V_{L,ax,max}} = -2 \left(\frac{r}{R} \right)^2 + 1 \quad \dots (3.14a)$$

This equation corresponds to a parabolic velocity profile where the maximum down flow velocity at the reactor edge equals the maximum up flow velocity in the reactor center.

The following form was considered for gas holdup radial distribution:

$$\varepsilon_G = \bar{\varepsilon}_G \left[\frac{n+2}{n} \right] \left[1 - \left(\frac{r}{R} \right)^n \right] \quad \dots (3.15)$$

Where $n = 2$ for an air-water system [Kelkar 1986].

3.9 Transition Regime

An increase in superficial gas velocity increases the centerline liquid axial velocity up to a maximum value, concluded that the maximum indicates the transition from homogeneous to heterogeneous flow. Because no gas holdup data was provided, it is not known whether the maximum in centerline axial velocity is due to the S-shaped gas holdup curve that might be present in their system [Franz *et. al.*, 1984].

However, when the change in slope is gradual or the gas holdup curve does not show a maximum in gas holdup, it is difficult to identify the transition point. In such cases, the drift flux method proposed by Wallis, (1969) has been used extensively.

In this method, the drift flux, j_{GL} (the volumetric flux of either phase relative to a surface moving at the volumetric average velocity) is plotted against the superficial gas velocity, u_G . The drift flux velocity is given by:

$$j_{GL} = u_G(1 - \varepsilon_G) \pm u_L \varepsilon_G \quad \dots (3.16)$$

Where ε_G is gas holdup and u_L is superficial liquid velocity. The positive or negative sign indicates counter-current or co-current flow of liquid relative to the gas phase, respectively. In the case of stationary liquid phase ($u_L = 0$) this equation simplifies to:

$$j = u_G(1 - \varepsilon_G) \quad \dots (3.17)$$

Figure (3.5) shows a typical plot of the drift flux versus gas holdup. The change in the slope of the curve represents the transition from homogeneous to heterogeneous flow. The change in slope of the drift flux plot is generally sharper than the change in slope of gas holdup curve.

The drift flux of gas increases with the gas holdup in the dispersed regime; in the coalesced bubble regime, the rate of increase is much larger.

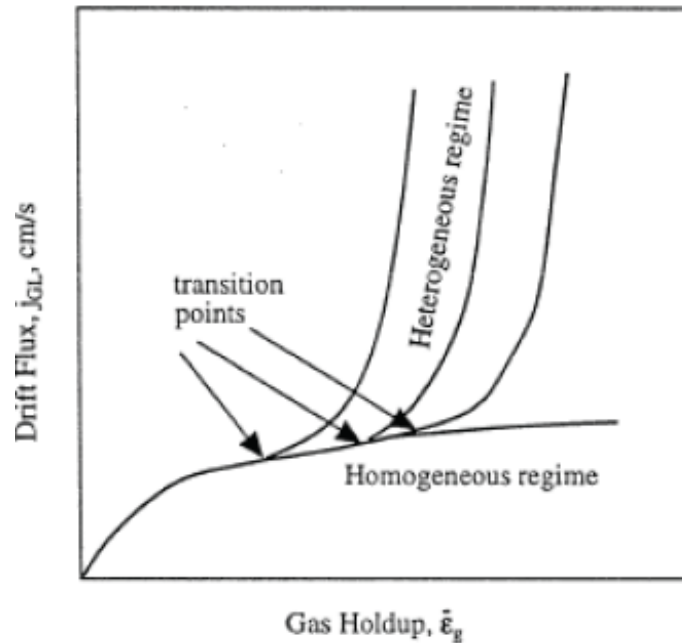


Figure (3.4) Typical drift flux plot using Wallis (1969) approach (Deckwer *et al.*, 1981).

The transition velocity depends on a number of factors such as gas distributor design, physical properties of the phases, and column size. The transition velocity is higher at higher system pressures and/or temperatures [Zhe Cui, 2005].

The following equations to predict transition velocity and holdup:

$$\frac{U_{tran}}{U_{s,b}} = \varepsilon_{tran} = 0.5 \exp(-193 \rho_G^{-0.61} \mu_L^{0.5} \sigma^{0.11}) \quad \dots (3.18)$$

$$\frac{U_{s,b} \mu_L}{\sigma} = 2.23 \left[\frac{\sigma^3 \rho_L}{g \mu_L^4} \right]^{-0.273} \left[\frac{\rho_L}{\rho_G} \right]^{0.03} \quad \dots (3.19)$$

Where $U_{s,b}$ is the rise velocity of the bubbles [Wilkinson *et al.*, 1992].

CHAPTER FOUR

RESULTS AND DISCUSSION

4.1 Computational Fluid Dynamics (CFD) Simulations

All the mentioned factors in chapter three which influence hydrodynamics of airlift reactors and bubble column greatly influence the liquid recurrent in the column. The simulations are the best way to study the gas holdup and liquid velocity in airlift reactors and bubble column because experimentation consuming time, costly, and it is difficult to separate effects of interdependent variables by testing. CFD simulations will allow variable affects to be studied and optimized before a system is designed and tested [Anderson, 2004].

4.2 Computing Technology

Rapid progress in three influencing technologies over the past two decades has brought CFD to the forefront of process engineering. Advances in computational technology, and sustained effort by CFD providers to implement comprehensive physical models, and advances in numerical methods have combined to make it possible for engineering to use CFD routinely in many process industrial companies [Haidari and Matthews, 2003].

ANSYS Inc., found in (1970) develops and globally markets engineering simulation software and technologies widely used by engineers and designers across abroad spectrum of industries. The company focuses on the development of open and flexible solutions that enable users to analyze design directly on the desktop, providing a common plate form for fast,

efficient and cost-conscious product development, from design concept to final-stage testing and validation.

CFX-5 includes a variety of multiphase models to allow the simulation of processes which transport and bring into direct contact multiple fluid streams to effect mixing, reaction, and separation. Multiphase flow in CFX-5 using Eulerian–Eulerian multiphase model. Two different sub-models are available for Eulerian-Eulerian multiphase flow:

- The Homogeneous Model: This is the simplest model, in which all fluids share the same flow field.
- The Inter-fluid Transfer or Inhomogeneous Model: Each fluid possesses its own flow field and the fluids interact via interphase transfer terms. Two different sub-models are available which differ in the way they model the interphase transfer terms. These are: the Particle Model and the Mixture Model [Wang *et. al.*, 2003].

4.3 Development of CFD Model

In present work Eulerian simulations were carried out for an airlift reactor using 3-D CFX-5, shown schematically in figure (4.1). This geometry corresponds to an experimental setup used by Baten *et. al.*, (1999) Consisting of a polyacrylate column with an inner diameter of 0.15 m and a length of 2 m. At the bottom of the column, the gas phase is introduced through a perforated plate with 108 holes of 0.5 mm in diameter. A polyacrylate draft tube (riser) of 0.10 m inner and 0.11 m outer diameter, with a length of 2.02 m, is mounted into the column 0.10 m above the gas distributor. A gas-liquid separator is mounted at the top of the column of 1 m in height and 0.38m in diameter. The main purposes of the separator of airlift reactors, where the riser and the downcomer interconnect, are the gas disengagement and avoid

gas flow in the downcomer section. This effect is usually achieved by increasing the cross-sectional area of the reactor head zone, where the reduce of a velocity of liquid flowing downwards into the downcomer occurs [Dolgos *et.al.*, 2001].

The superficial gas velocity, U_G , at the bottom inlet was varied in the range 0.018634-0.11419 m/s. the physical and transport properties of the gas and liquid phases are specified in table (4.1)

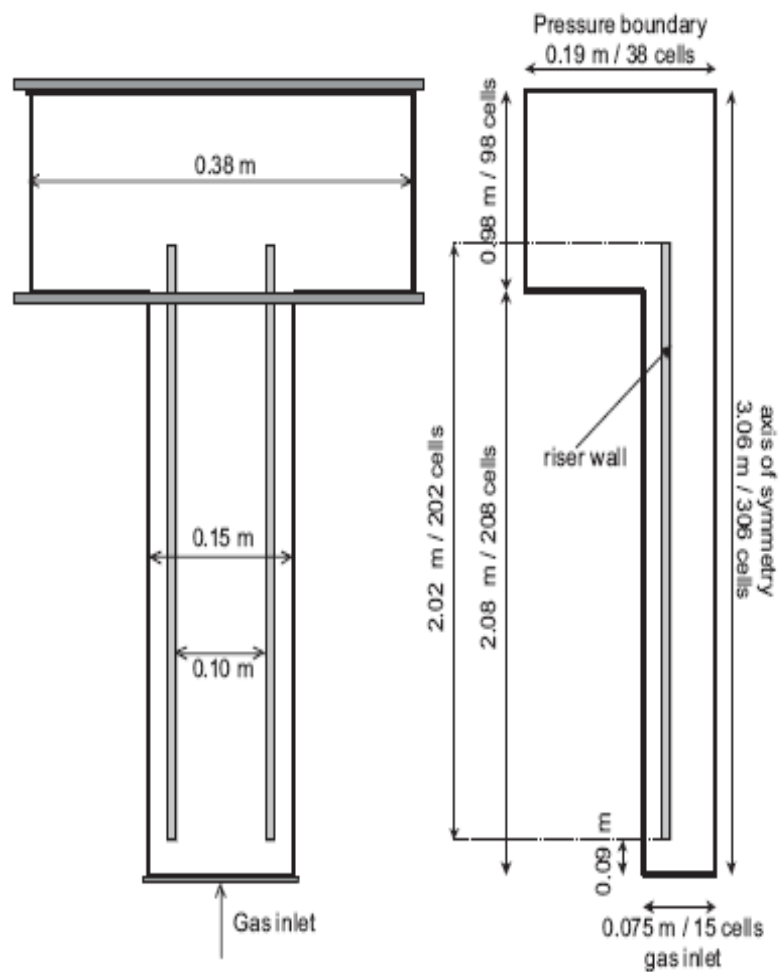


Figure (4.1) schematic diagram of airlift reactor, showing the computational domains and grid details.

4.4 Simulation Results

Recent publications have shown that hydrodynamics of airlift reactors and bubble column can be estimated with computational fluid dynamic simulations based on Eulerian equations. The results of the simulations are close to experimental results of Baten *et. al.*, (1999). Following snap-shots show the 3D axis-symmetric simulations results for gas holdup and liquid velocity at different superficial gas velocities. The colors depict gas holdup and liquid velocity according to the scale shown on the left.

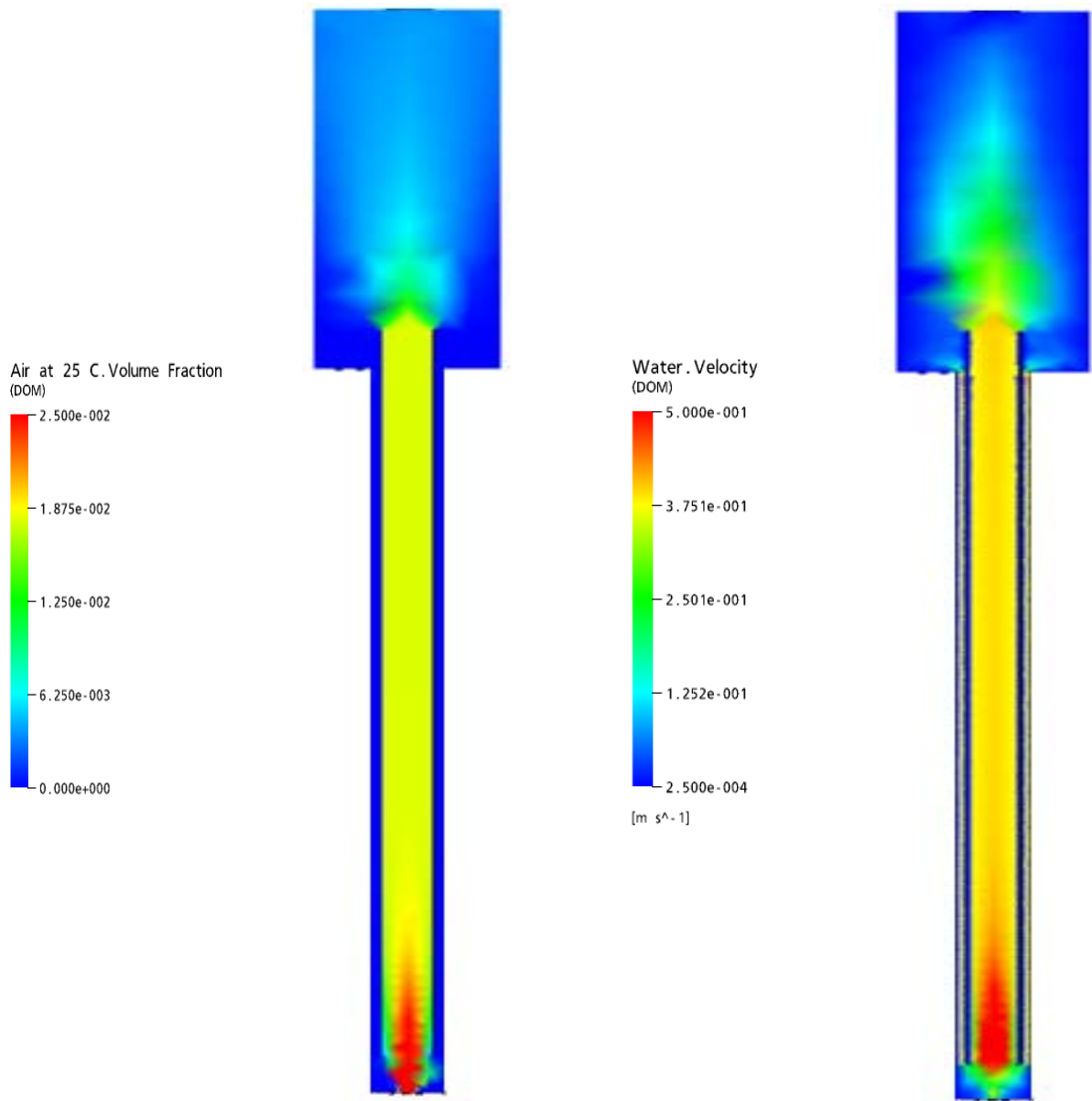


Figure (4.2) Contours of air volume fraction and liquid velocity at 0.018634 m/s superficial gas velocity.

Table (4.1) Local and average gas holdup and liquid velocity in riser and downcomer at 0.018634 m/s superficial gas velocity.

$Z \text{ (m)}$	$\varepsilon_r \text{ (-)}$	$V_{Lr} \text{ (m/s)}$	$V_{Ld} \text{ (m/s)}$
0.1	0.0372094	0.657394	0.35544
1	0.01781	0.394913	0.363036
2	0.0178034	0.396347	0.286648
avg.	0.024274	0.482885	0.33501133

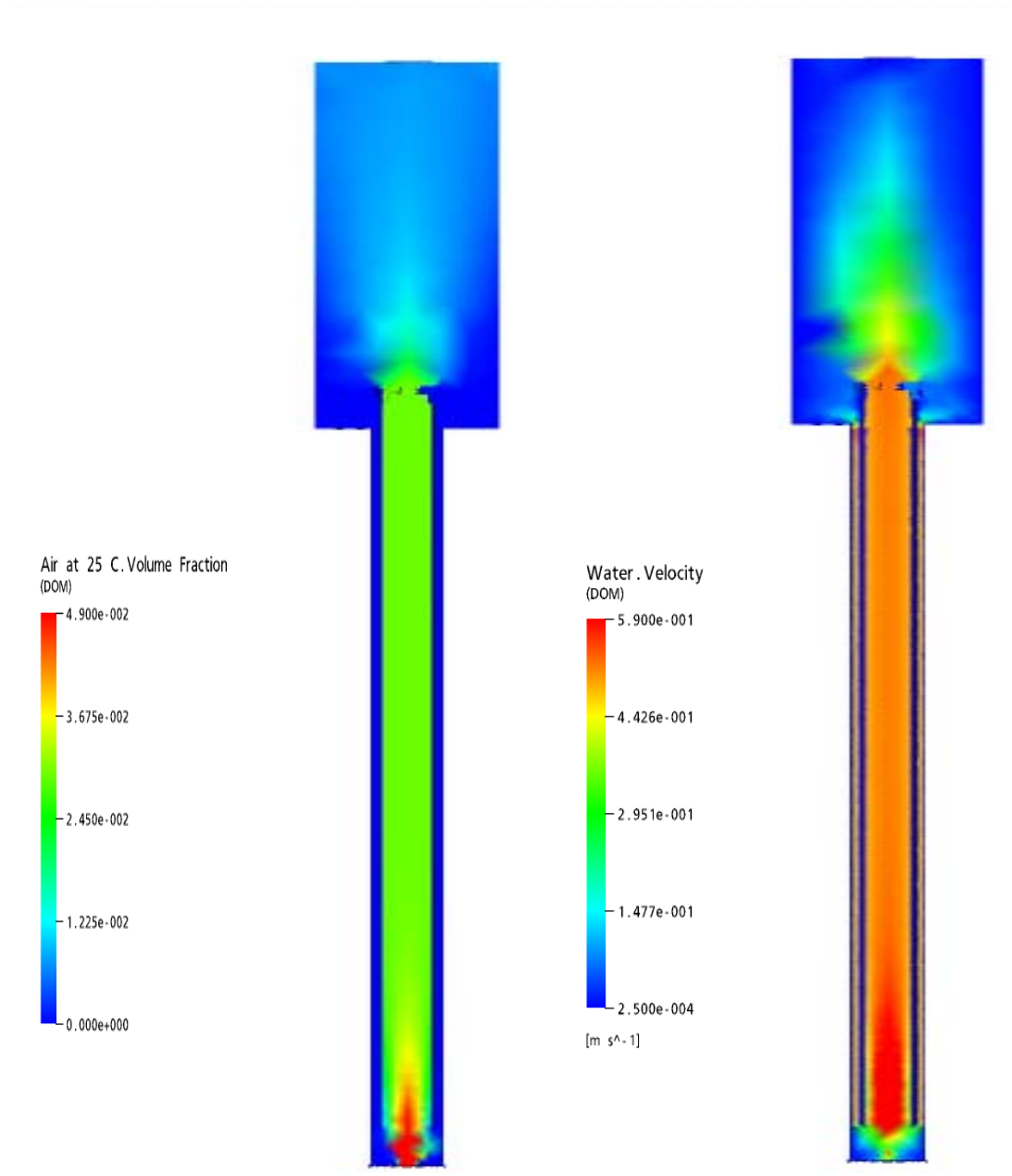


Figure (4.3) Contours of air volume fraction and liquid velocity at 0.040887m/s superficial gas velocity.

Table (4.2) Local and average gas holdup and liquid velocity in riser and downcomer at 0.040887m/s superficial gas velocity.

$Z \text{ (m)}$	$\epsilon_r \text{ (-)}$	$V_{Lr} \text{ (m/s)}$	$V_{Ld} \text{ (m/s)}$
0.1	0.0884672	0.616815	0.47503
1	0.0295163	0.520283	0.503896
2	0.0295413	0.521975	0.541629
avg.	0.049175	0.553024	0.50685167

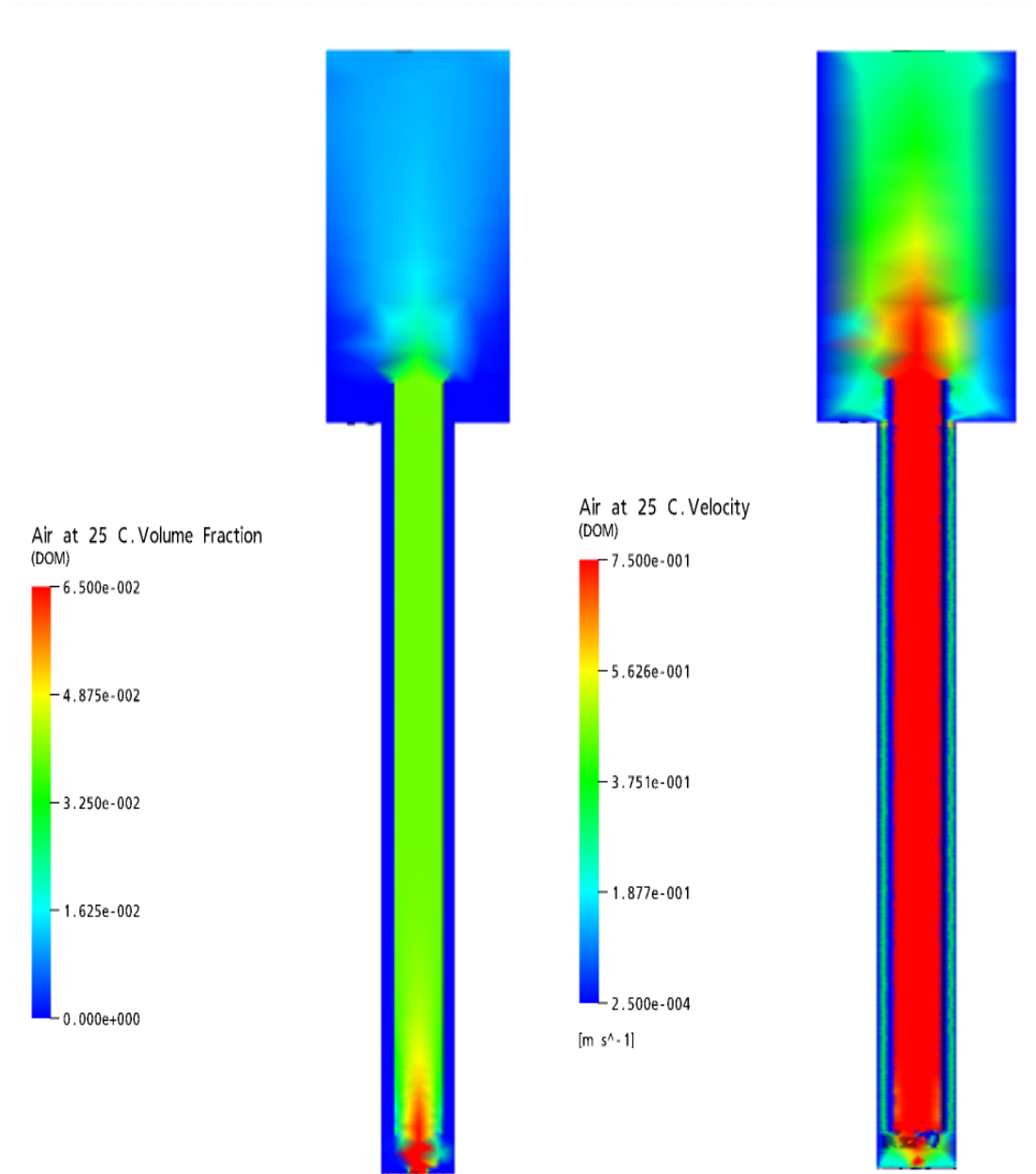


Figure (4.4) Contours of air volume fraction and liquid velocity at 0.056583 m/s superficial gas velocity.

Table (4.3) Local and average gas holdup and liquid velocity in riser and downcomer at 0.056583 m/s superficial gas velocity

$Z \text{ (m)}$	$\varepsilon_r \text{ (-)}$	$V_{Lr} \text{ (m/s)}$	$V_{Ld} \text{ (m/s)}$
0.1	0.112575	0.731662	0.55421
1	0.039509	0.611668	0.552622
2	0.0395456	0.613645	0.629912
avg.	0.063877	0.652325	0.578915

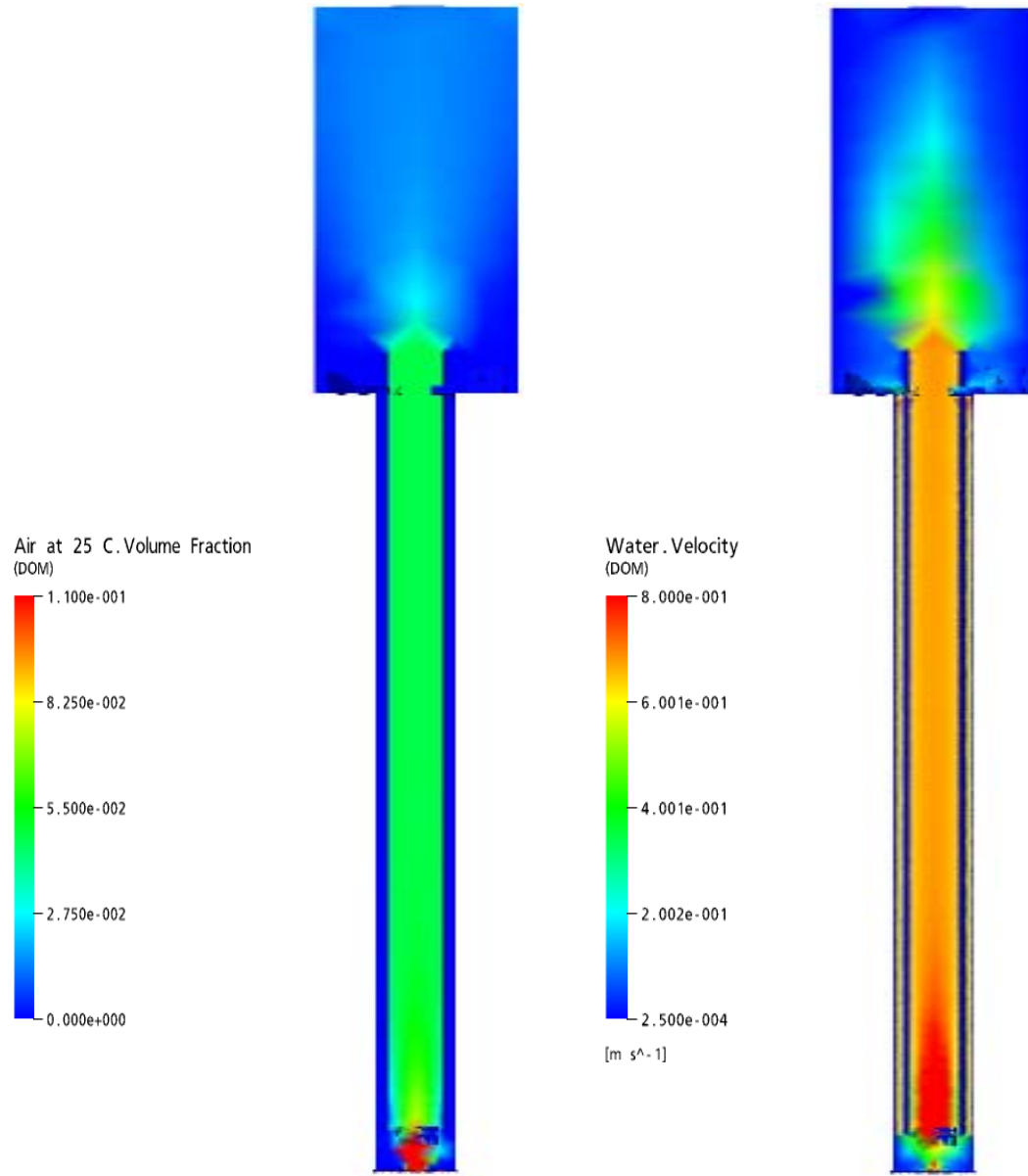


Figure (4.5) Contours of air volume fraction and liquid velocity at 0.081263 m/s superficial gas velocity.

Table (4.4) Local and average gas holdup and liquid velocity in riser and downcomer at 0.081263 m/s superficial gas velocity.

$Z \text{ (m)}$	$\varepsilon_r \text{ (-)}$	$V_{Lr} \text{ (m/s)}$	$V_{Ld} \text{ (m/s)}$
0.1	0.226003	0.820894	0.843834
1	0.0475058	0.679565	0.608293
2	0.0475274	0.681273	0.608037
avg.	0.107012	0.727244	0.68672133

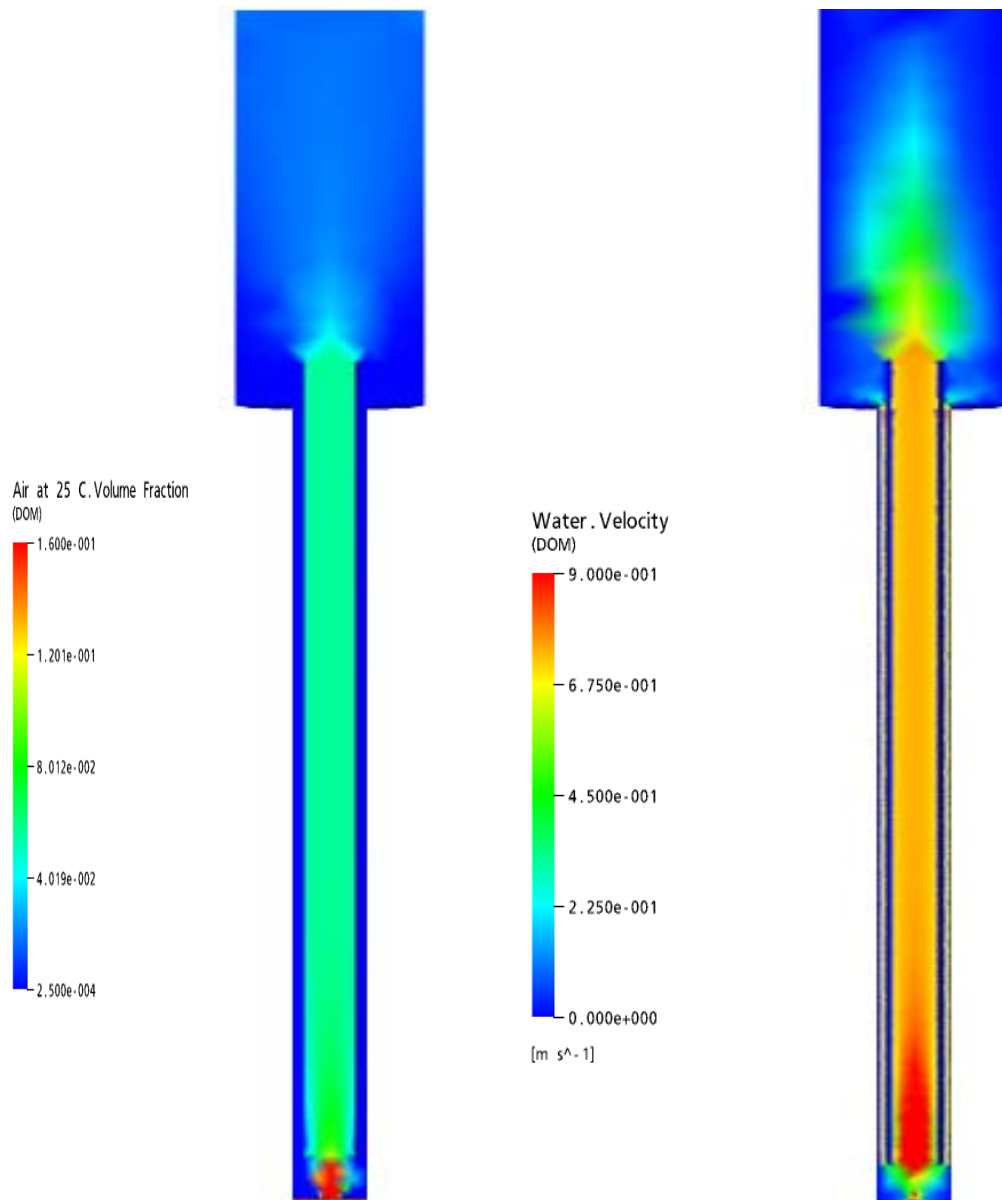


Figure (4.6) Contours of air volume fraction and liquid velocity at 0.094986 m/s superficial gas velocity.

Table (4.5) Local and average gas holdup and liquid velocity in riser and downcomer at 0.094986 m/s superficial gas velocity.

$Z \text{ (m)}$	$\varepsilon_r \text{ (-)}$	$V_{Lr} \text{ (m/s)}$	$V_{Ld} \text{ (m/s)}$
0.1	0.14587	1.02717	0.650174
1	0.0566792	0.7488	0.665559
2	0.0566638	0.750821	0.731122
avg.	0.086404	0.842264	0.682285

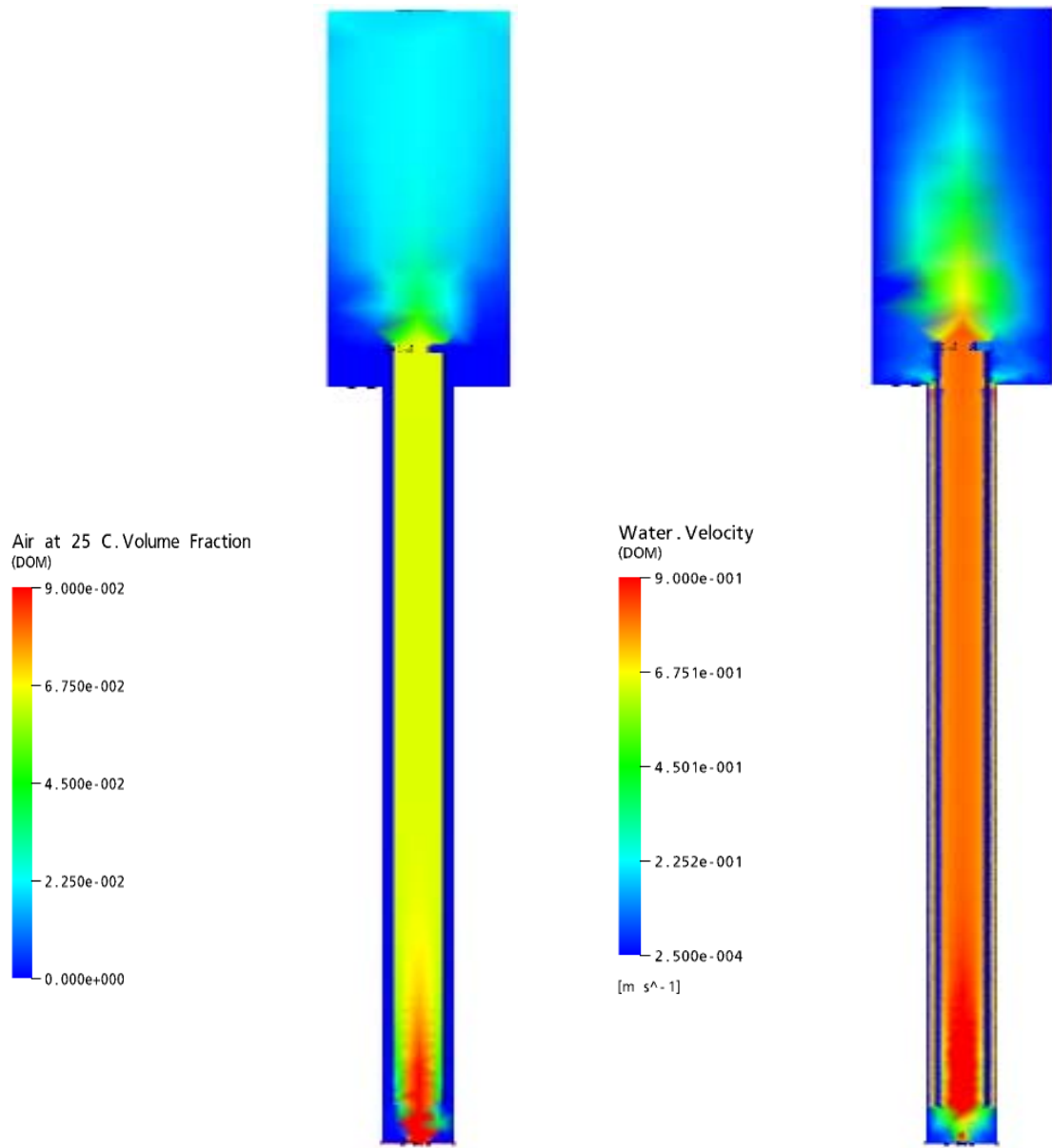


Figure (4.7) Contours of air volume fraction and liquid velocity at 0.11419193 m/s superficial gas velocity.

Table (4.6) Local and average gas holdup and liquid velocity in riser and downcomer at 0.11419193 m/s superficial gas velocity.

$Z \text{ (m)}$	$\varepsilon_r \text{ (-)}$	$V_{Lr} \text{ (m/s)}$	$V_{Ld} \text{ (m/s)}$
0.1	0.136981	1.2097	0.711188
1	0.064201	0.806159	0.711464
2	0.064292	0.818294	0.939554
Avg.	0.088491	0.944718	0.787402

4.5 Mechanism of Flow in Airlift Reactor

From figures (4.2-4.3-4.4-4.5-4.6 and 4.7) contours 3D axis-symmetric observe in the riser, gas injection produces a highly turbulent region with high gas holdup. In the downcomer, the liquid returns to the bottom after separating from the gas bubbles that disengage in the gas separator. A fraction of gas may eventually be entrapped in the downcomer, depending on the airlift reactor geometry and operating conditions. The gas holdup, however, remains lower than that in the riser, and the difference in the gas holdups between the two regions produces the difference in the apparent fluid density that drives the liquid circulation. The circulating liquid flow enhances the heat transfer and makes the liquid properties homogeneous in the column. In terms of gas-liquid flow configurations, in the riser and separator bubbly or bubbly turbulent flow observed. In the downcomer, the liquid will usually show a near-plug-flow behavior; as long as the tubes are vertical.

Bubble size itself has of important influence for all flow processes in the reactor; setting it to a constant value means neglecting all effects of coalescence, bubble-breakup and expansion due to hydrostatic pressure decrease with increasing vertical position in the reactor and thus can be held responsible for the model's actual inability to account for the flow regime transitions observed in the measurements.

Figure (4.8) shows gas holdup in the riser and average liquid velocities in the riser and downcomer increases with increasing the superficial gas velocity. the results obtained from airlift simulations compared with experimentally determined values by Van Baten *et al.*, (1999), there is very good agreement between them.

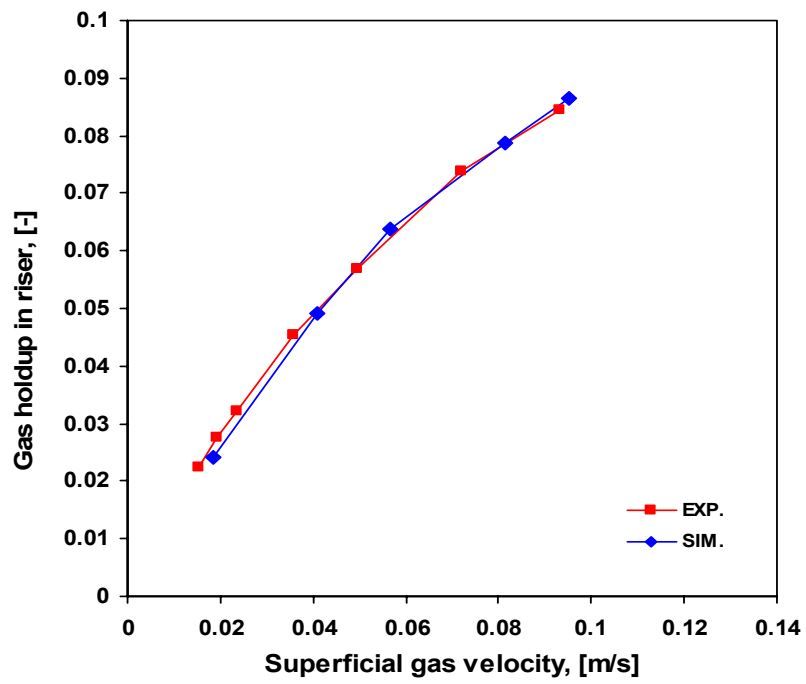


Figure (4.8a) average gas holdup in the riser

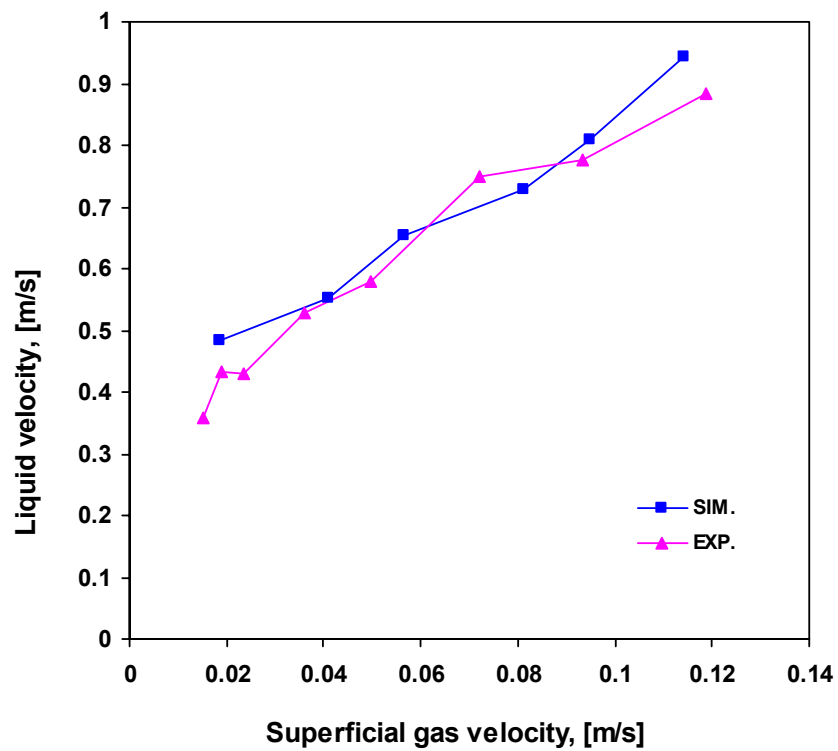


Figure (4.8b) Average liquid velocity in the riser

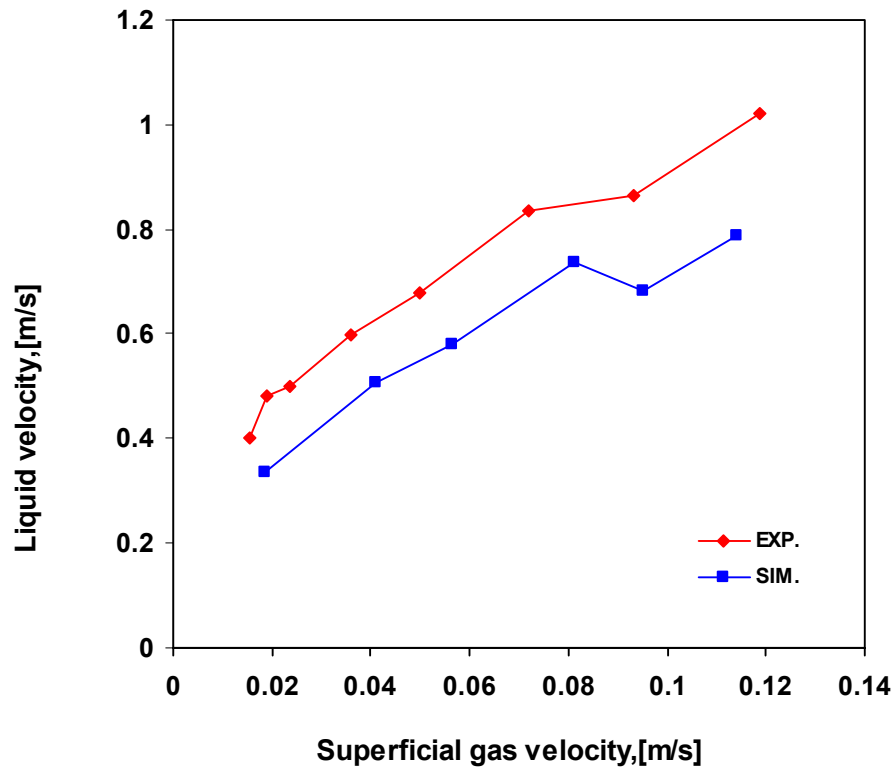


Figure (4.8c) average liquid velocity in the downcomer

In figure (4.8a, b) the gas and liquid velocities can be considered to flow up the riser virtually in plug flow. With increasing superficial gas velocities, the liquid velocities start to assume a parabolic profile. Within the central core of the riser, the gas holdup profiles are nearly uniform for the whole range of superficial gas velocities (u_G) values.

Figure (4.8b) presents the vertical velocity in the riser against the superficial gas velocity in the riser. The trend of the experimental data is that of rapidly rising velocity up to 0.02 m s^{-1} of the superficial gas velocity in the riser. Then there is a reduction in the rate of change of the velocity as the turbulent flow effects begin to influence the gas phase motion for superficial gas velocity in the riser greater than 0.02 m s^{-1} . This change in the velocity profile is also observed in the simulated data at 0.02 m s^{-1} but more data

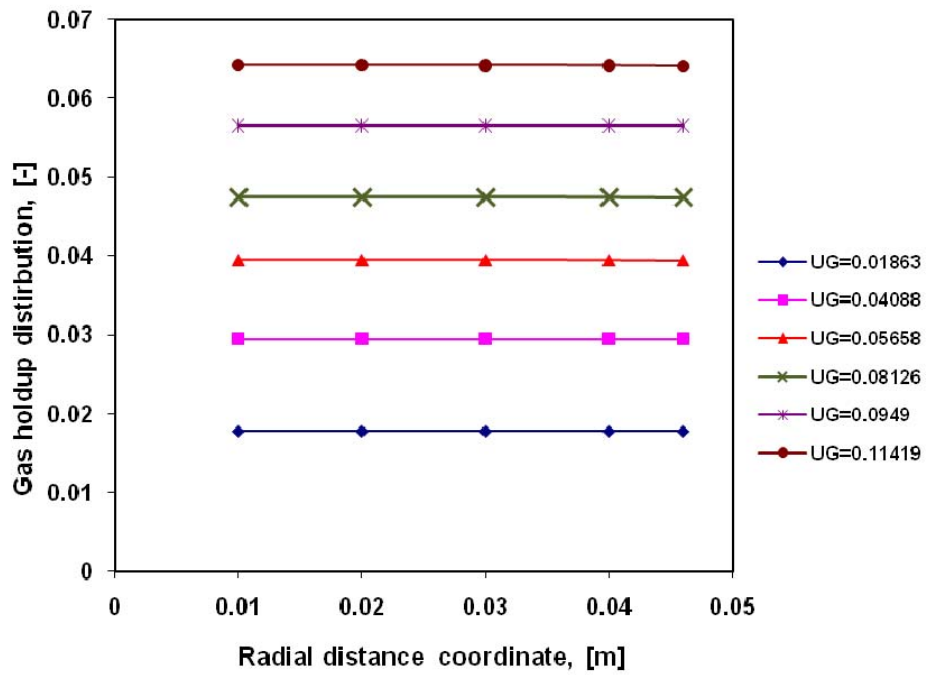
points are required below this value to confirm the change. But generally the profile of the simulated data fits the empirical profile.

Figure (4.8c) presents the liquid phase velocity in the downcomer. The flow regime changes as the influence of turbulent flow effects increase. The simulated data consistently over-predicts the liquid velocity and though the profile is not linear, more data is required for the lower range of superficial gas velocities is required to confirm this effect. Because of the presence of separator, the gas holdup in downcomer approximately broke. Therefore the reduction appears in the accuracy of the flow data of simulation between the riser and downcomer. and also There are three effects in the model used that could influence the accuracy of the simulation in the downcomer, the use of a single gas fraction of a mean bubble size, the volume fraction equation formulation and the resolution of the mesh in the downcomer.

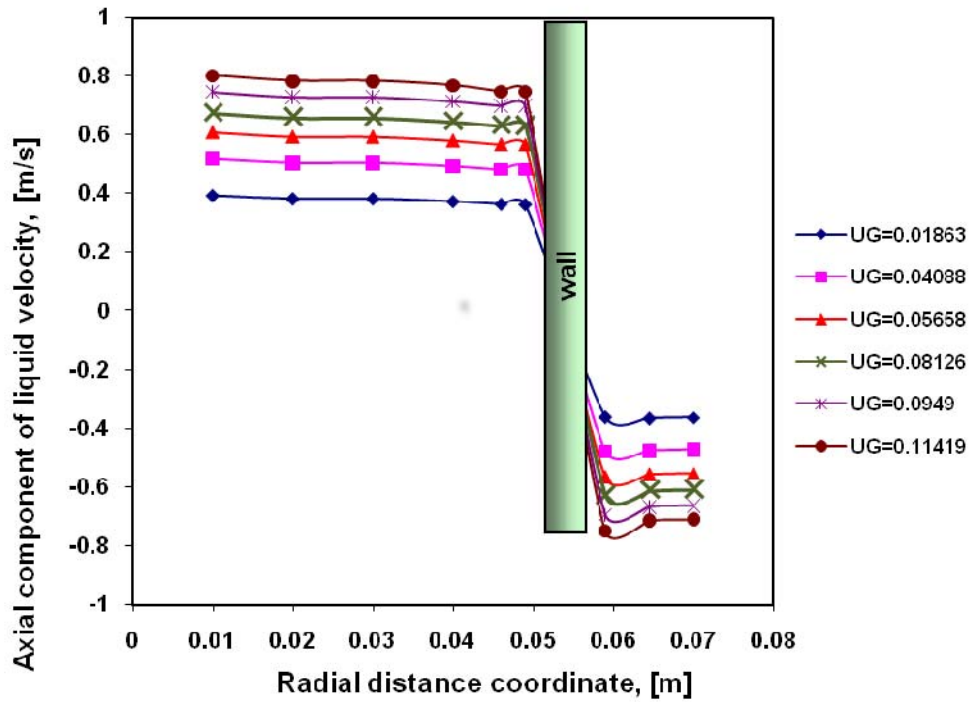
4.6 Radial Distribution

The results in figure (4.9a, b) shows radial distribution of gas holdup and the axial liquid velocity in riser and downcomer, for varying superficial gas velocity, at height 1.75m above the sparger.

The increase rate varies with gas velocity, Unlike the radial distribution liquid velocity increases slowly with increasing gas velocity at low gas velocities as shown in figure (4.9a, b). It is due to the fact that at lower superficial gas velocities, the airlift reactor is in bubbling regime, bubble size is smaller and more uniform, and the gas holdup is more uniform, so the increase of superficial gas velocity will not affect the liquid axial velocity too much.



(a) Gas holdup distribution



(b) Liquid velocity distribution

Figure (4.9) Radial distribution of: a) Gas holdup b) liquid velocity in riser and downcomer, for varying superficial gas velocity, at height 1.75m above the sparger

4.7 Transition Velocity

Figure (4.10) shows the effect of gas velocity on the axial liquid velocity at the column center.

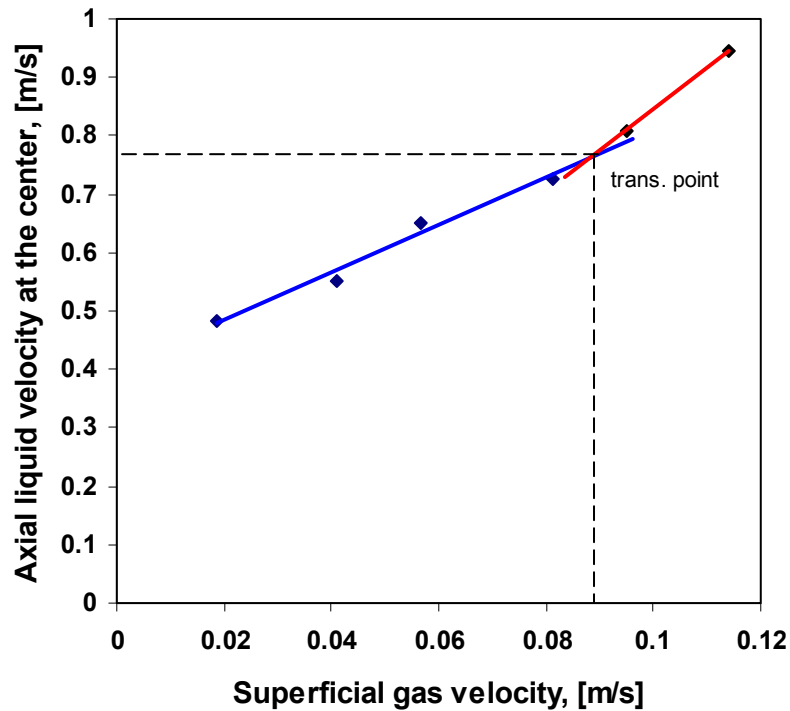


Figure (4.10) Effect of gas velocity on the axial liquid velocity at column center.

The axial liquid velocity at the center point increases with an increase in the superficial gas velocity, however, the increase rate varies with gas velocity. At low gas velocities, the central liquid velocity increases quickly with superficial gas velocity. The increase rate of center liquid velocity with gas velocity becomes smaller. The point that the increase rate suddenly changes can be defined as the flow regime transition point.

4.8 Transition Regime Identification Using the Drift Flux Plot

The transition gas holdup and superficial gas velocity identified using the drift flux plot, as shown in figures (4.11) and (4.12).

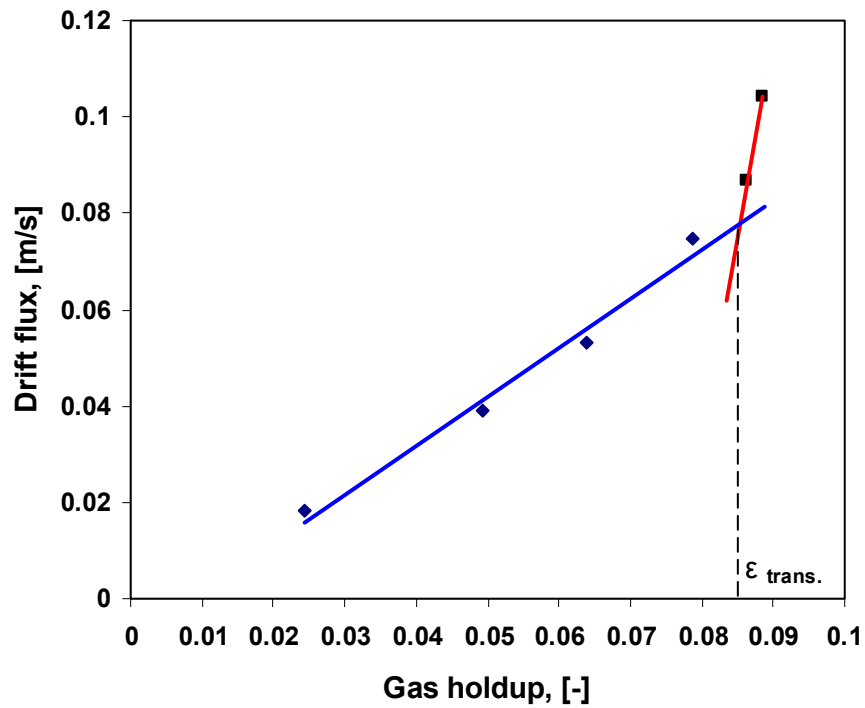


Figure (4.11) Identification of flow regime transition based on drift-flux method.

When the drift flux is plotted against the gas holdup, the change in the slope of the curve indicates the transition from homogeneous region to the heterogeneous region.

Figure (4.11) shows the relation between the drift-flux and the gas holdup. The transition velocity obtained based on the drift-flux method is about 0.085 m/s as shown in figure (4.12).

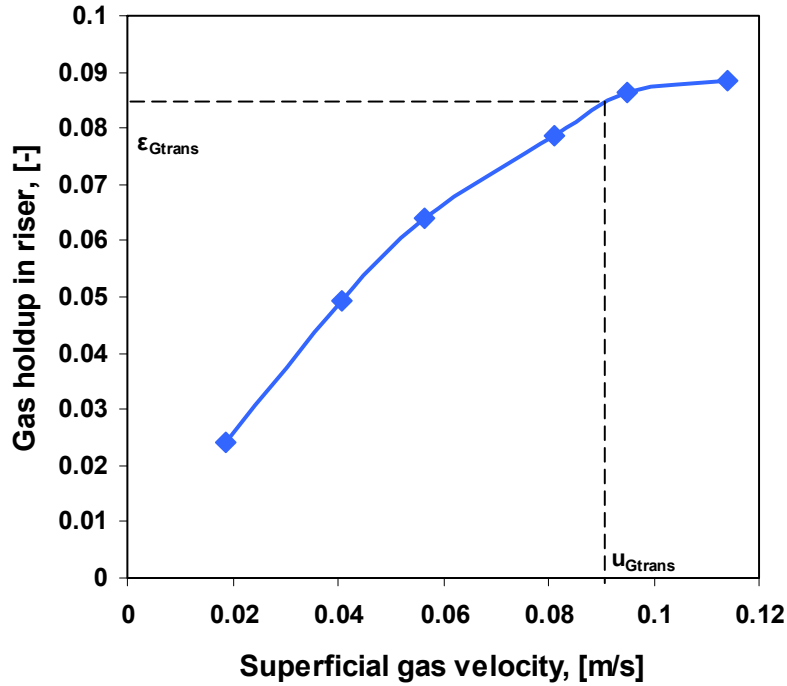


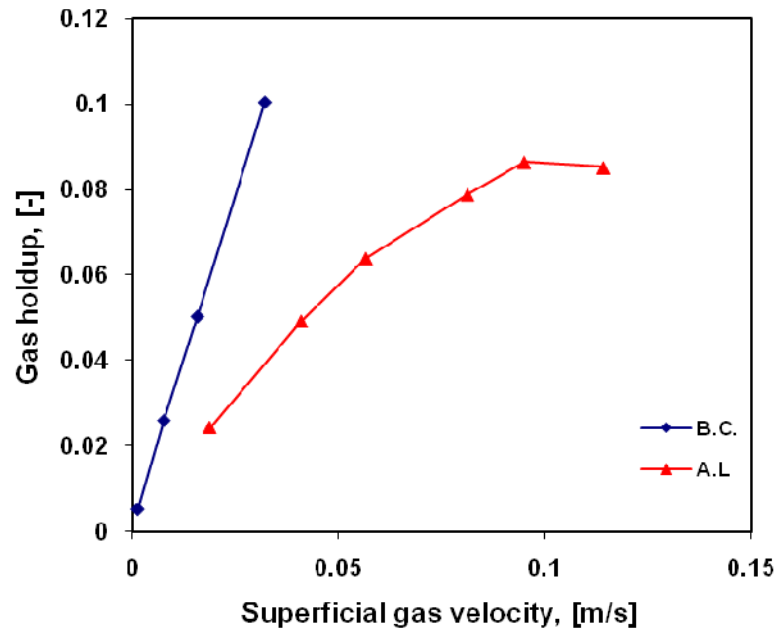
Figure (4.12) Effect of superficial gas velocity on the gas hold-up in riser of airlift reactor ($U_{G,trans} = 0.0899$ m/s).

4.9 Comparisons between the Hydrodynamics in the Airlift reactor with Bubble Columns

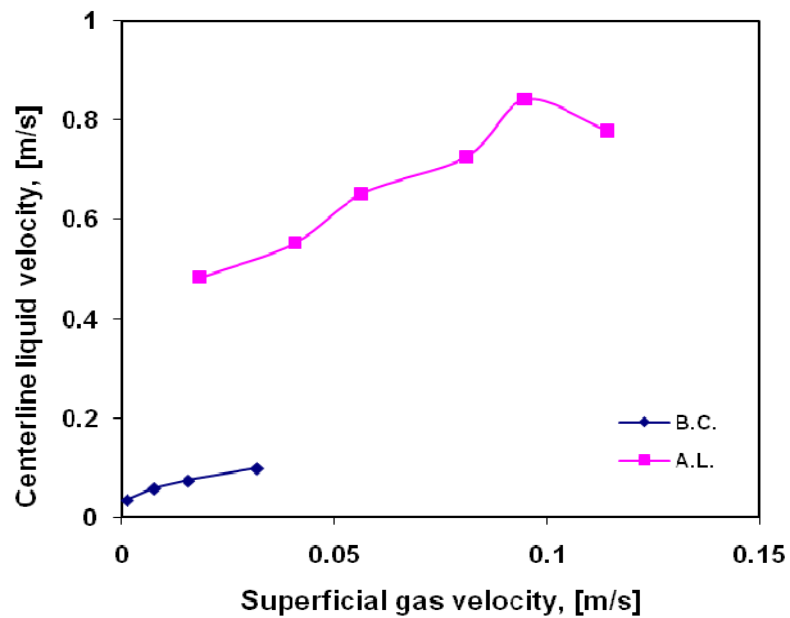
Figure (4.13a, b) shows comparison between the gas holdup and liquid velocity profiles in the airlift reactor with corresponding results in bubble columns of diameter 0.15 m. The superficial gas velocity, U_G , for the airlift is defined in term of the riser cross-sectional area and the gas holdup is the global value in the system.

The gas holdup in the airlift is significantly lower than for bubble column, this is because of the much lower slip velocity between the gas and liquid phases within the riser of the airlift. The lower slip is due to much higher liquid circulation. The centerline liquid velocity within the riser, or

bubble column, V_L was taken as a measure of the circulation; the values for the airlift are compared with bubble columns in figure (4.13b).



(a) Gas holdup



(b) Centerline liquid velocity

Figure (4.13) Comparison of: (a) gas holdup and (b) centerline liquid velocity, $V_L(0)$, for airlift reactor with bubble column of 0.15 m diameter

The bubble column simulation results presented in figure (4.13) are restricted to U_G values below 0.04m/s because for higher value of U_G the heterogeneous or churn-turbulent regime of operation is entered into [Baten and Krishna, 2002] as shown in figures (4.14) and (4.15) .

The airlift reactor can be operated at U_G values up to 0.12 m/s while maintaining the homogenous bubble flow regime since the effective slip velocity in the riser is much lower. The ability to operate in the homogeneous bubble flow regime till much higher superficial gas velocities than bubble column is major advantage of the airlift reactors.

Figures (4.14) and (4.15) show the flow regimes of bubble column of diameter 0.15 m using drift flux method.

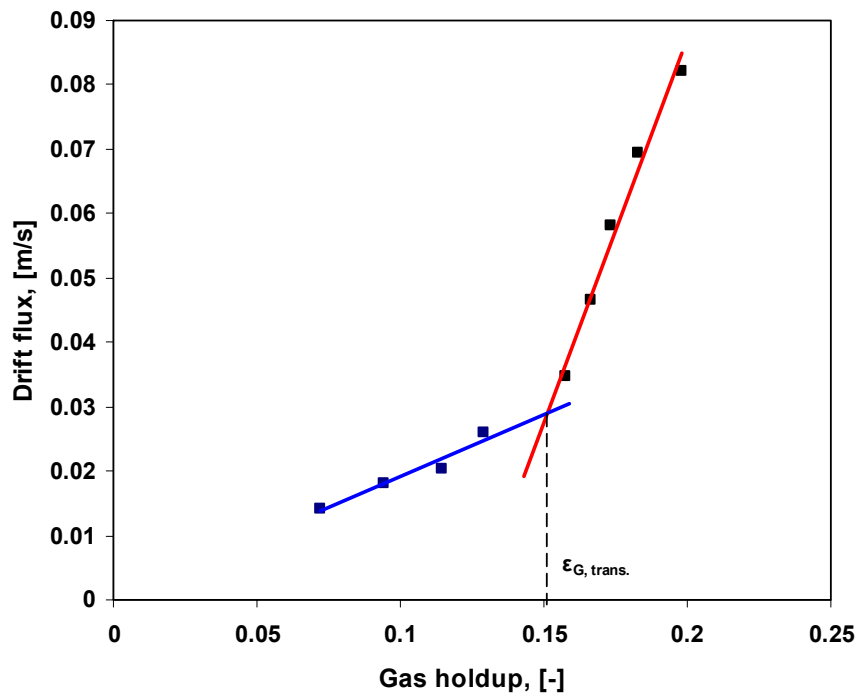


Figure (4.14) Identification of flow regime transition based on drift-flux method in bubble column of 0.15 m diameter.

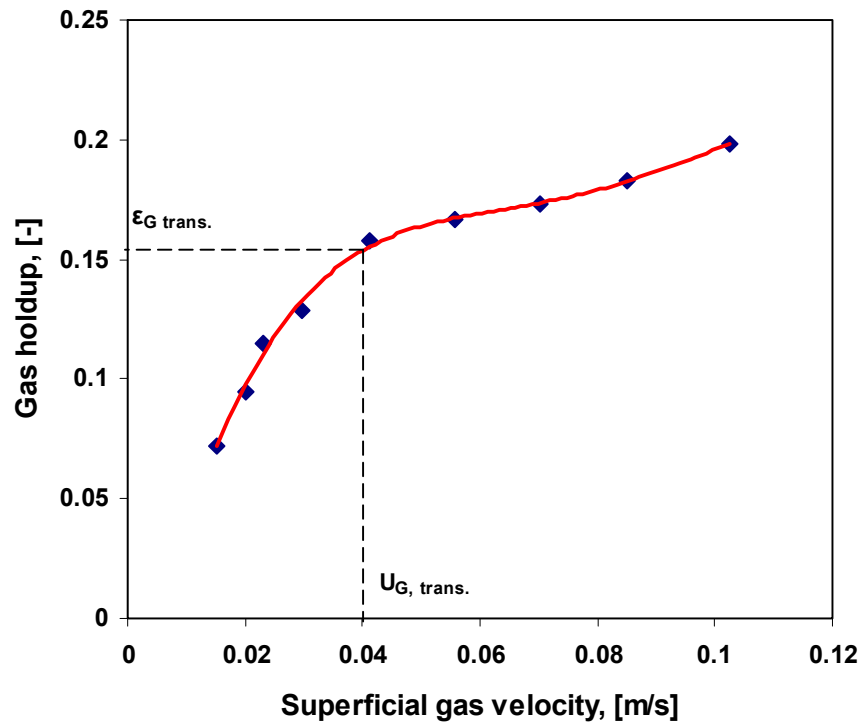


Figure (4.15) Effect of superficial gas velocity on the gas hold-up in riser of bubble column of diameter 0.15 m ($U_{G,trans} = 0.04$ m/s).

At a low superficial gas velocity, the bubbles rise independently with fairly uniform spacing between them. The flow pattern shows mostly random short range eddies. The lowest superficial gas velocity of transition regime correspond to the point where overall gas-holdup breaks away from the ideal curve for uniform bubble flow to transition flow is asymptotic, depending on various factors, which effect the size of gas bubble by altering the degree of coalescence-suppressing condition the most evident features observed are that the uniform bubble swarm begins to minder, indicating an accuracy of local liquid circulation near the side wall in bubble column and in downcomer of airlift reactor. With increasing U_G , bubble clusters begins to appear in the bulk of column, and gross and local liquid circulation, i.e. turbulences in the liquid flow, develop randomly in space and time.

In loop reactors, the regime transitions can be delayed up to much higher superficial gas velocities, because of the effect of the overall liquid velocity on the stability of the flow. The differences between regimes are less apparent in airlift reactors as compared to bubble columns, due to the opposite effects mentioned above.

CHAPTER FIVE

Conclusions and Recommendation for Future Work

5.1 Conclusions

The following conclusions could be drawn from the work:

1. The gas and liquid phases show virtual plug flow behavior in the riser of an airlift. This is contrast with bubble columns where both gas and liquid phases deviate strongly from plug flow.
2. Due to the much lower slip between gas and liquid velocities in the riser of the airlift, homogenous bubble flow can be maintained at much higher U_G values in airlifts than in bubble columns.
3. CFD simulation can be powerful tool for the modeling and design of airlift and bubble column reactors, especially in the context of describing the complex flow of the gas and liquid phases for different geometrical configurations.
4. The transition regimes appears at high superficial gas velocity in airlift reactors because of its ability to operate in the homogeneous bubble flow regime till much higher superficial gas velocities than bubble column is major advantage of the airlift reactors
5. Liquid flow velocities clearly showed the influence of superficial gas velocity on liquid circulation in the reactor. The common radial profile of axial liquid velocity far away from sparger and degassing zone influence exhibits a parabolic to almost linear shape with an upflow maximum in the center and a down flow region in down comer.

5.2 Recommendations for Future Work

From the present study, it is noticed that further studies in the following areas would be desired:

1. The effect of type of sparger on the gas holdup and liquid velocity.
2. The hydrodynamics of airlift reactors at high superficial gas velocity in the riser.
3. Mixing in the airlift reactors.
4. Comparison of the hydrodynamics of internal and external loop in airlift reactors.
5. The effect of using high liquid viscosity instead of water.
6. The effect of electrolyte and solid suspension on hydrodynamics of airlift reactors.

REFERENCES

1. Abid Akhtar, Pareek, V., K., and Tade, M., O., " Modern Trends in CFD Simulations: Application to GTL Technology", Chem. Prod. and Process Modeling, Vol. 1, Issue 1, Article2, 2006.
2. Anderson, G., D., P., "Analysis of Currents and Mixing in a modified Bubble Column Reactor", the Canadian society for engineering in agricultural food, and biological system, no. 043071, 2004.
3. Baten, V. J. M., Krishna, R., Chem. Eng. Technol, 25, 1081, 2002.
4. Baten, V., J.M., and Krishna, R., " Comparison of hydrodynamic and Mass Transfer in Airlift and Bubble Column Reactors Using CFD", Chem. Eng. Techno, pp. (1047-1079), 2003.
5. Blazej, M., Glover, C., G.M., Generalis, S.C., and Markos, J., "Gas–Liquid Simulation of an Airlift Bubble Column Reactor", Chem. Eng. and Processing 43, 137–144, 2004.
6. Bohn, M., S., "First 3D Simulation of Bubble Column Hydrodynamics Paves Way for Commercial Gas-to-Liquid Conversion in Slurry Reactor", Vice President, Engineering, 2000.
7. Buwa, V., and Ranade, V., "Bubbling Columns", National chemical laboratory, India, 2003.
8. Chen, R.C., Fan, L.-S., "Particle image velocimetry for characterizing the low structure in three-dimensional gas-liquid-solid fluidized beds, 1992.

9. Chen, R.C., Reese, J., and Fan, F.-S., "Flow Structure in a Three-Dimensional Bubble Column and a Three-Phase Fluidized Bed", *AIChE J.*, 40(7): 1093-1104, 1994.
10. Chisti and Molina, "A reassessment of relationship between riser and down comer gas holdups in airlift reactors ", *Chem. Eng. Science*, Vol. 53, No.24, pp.4151-4154, 1998.
11. Chemical Industry of the Future Technology Roadmap for Computational Fluid Dynamics, 1999.
12. Dautzenberg, F., M., and de Deken, J., C., "Reactor developments in hydrotreating and conversion of residues", *Catal. Rev. Sci. Eng.*, **26**, 421, 1984.
13. Deckwer, W.-D., (1992): *Bubble Column Reactors*, J. Wiley & Son LTD, Chichester.
14. Deen, N.G., Solberg, T., and Hjertager, B.H., "Numerical Simulation of the Gas-Liquid Flow in a Square Cross sectioned Bubble Column", <http://hugin.aue.auc.dk>, 2000.
15. Delmas, H., Helene Chaumat, H., and Billet, A., "Axial and Radial Investigation of Hydrodynamics in a Bubble Column; Influence of Fluids Flow Rates and Sparger Type", *International Journal of Chem. Reactor Eng.*, Vol. 4 2006 Article A25

- 16.Devanathan, N., "Investigation of Liquid Hydrodynamics in Bubble Columns via Computer Automated Radioactive Particle Tracking (CARPT) Facility", D.Sc. Thesis, Washington University, St. Louis, Missouri, USA , 1991.
- 17.Diaz, E., M., Montes, F., J., and Galan, **M.**, A.," Gas Liquid Flow in A rectangular Partially Aerated Bubble Column:-Combined Effect Aspect Ratio and Superficial Gas of Velocity", University of Salamanca, Salamanca, Spain, 2006.
- 18.Dolgos, O., Klein, J., Vicente, A., A., Teixeira, J., A., "Behavior of dual gas-liquid separator in an internal-loop airlift reactor –effect of top clearance", 28th Conference SSCHE, 21 – 25 May, 2001.
- 19.Fan, L.-S., Luo, X., Tsuchiya, K., Lin, T.-S., Chen, Q., and Lee, D. J., "Progress in Understanding the Fluid Dynamics of Bubble Column Reactors – II", Department of Chemical Engineering, The Ohio State University 140 W. 19th Ave., Columbus, Ohio 43210 USA, 1998.
- 20.Franz, K., Borner, T., Kantoreck, H., and Buchholz, R., "Flow structure in bubble columns", Ger. Chem. Eng., 7, 365-374, 1984.
- 21.Geary, N.W. and Rice, R.G., "Bubble Size Prediction for Rigid and Flexible Spargers ", AIChE J., Vol. 37, No. 2, pp.161-168, 1991 b.
- 22.Haidari, A., H., and matthews, "Future trends for computational fluid dynamics in the process industry", third international conference on CFD in the minerals and process industries, pp. (331), 2003.

23. Idogawa, K., Ikeda, K., Fukuda, T., and Morooka, S., Chem. Eng. Comm., 59, 201, 1987.
24. Hills, J.H., "Radial Non-uniformity of Velocity and Voidage in a Bubble Column", Trans. Inst. Chem. Eng., 52: 1-9 , 1975.
25. Joshi, J.B., Vitankar, V.S., Kulkarni, A.A., Dhotre, M.T., and Ekambara, K., "Coherent Flow Structures in Bubble Column Reactors", Chem. Eng. Science, Vol. 57, pp. 3157-3183, 2002.
26. Kawase, Y.; Moo-Young, M., "Liquid Phase Mixing in Bubble Columns with Newtonian and Non-Newtonian Fluids", Chem. Eng. Science 41, 1986.
27. Kelkar, Balmohan, G., "Flow regime characteristics in cocurrent bubble column reactors. Chemical Engineering Communications, 41(1-6), 237-251, 1986.
28. Klein, J., Vicente, A., A., and Teixeira, J., A., "Hydrodynamics of a Three-phase Airlift Reactor with an Enlarged Separator – Application to High Cell Density Systems", The Canadian Journal of Chemical Engineering, Volume 81, August 2003 .
29. Krishna, R. and Baten, J. M. V., "Mass transfer of bubble columns", Catalysis Today. 79- 80: 67-75, 2003.

30. Krishna, R., Urseanu, M. I., Baten, J. M. V., and Ellenberger, J., "Wall effects on the rise of single gas bubbles in liquids" *Int. Comm. Heat Mass Transfer*. 26(6): 781-790, 1999.
31. Kumar, D., "Design and Scale-Up of Bioreactors Using Computer Simulations", *Bioprocess International*, 2006.
32. Kuzmin, D., and Turek, S., "Efficient numerical techniques for flow simulation in bubble column reactor", University of Dortmund Vogelpothsweg 87, D-44227 Dortmund, Germany, 1999.
33. Gobby, D., Hamill, I. S., Jones, I. P., Lewin, J., and Montavon, C., "Application of CFD to Multi-Phase Mixing", CFX, AEA Technology Engineering Software, 2002.
34. Lain, S., Broder D., and Sommerfeld, M., "Numerical Modeling of the Hydrodynamics in a Bubble Column Using the Euler-Lagrange Approach", Universität Halle-Wittenberg, D-O6099 Halle (Saale). Germany, 2000.
35. Michele, V., "CFD Modeling and Measurement of Liquid Flow Structure and Phase Holdup in Two- and Three-Phase Bubble Columns", der Technischen Universität Carolo-Wilhelmina zu Braunschweig, 2001.
36. Marchot, P., Fransolet, E., L'Homme, G., Crine, M., and Toye, D., "Gas Liquid Solid Bubble Column Investigation by Electrical Resistance Tomography", Laboratoire de Génie Chimique, B6, Université de Liège, Liège B4000, Belgium, 2002.

37. Marchot, P., Fransolet, E., L'Homme, G., Crine, M., and Toye, D., "Gas Liquid Solid Bubble Column Investigation by Electrical Resistance Tomography", Université de Liège, Liège B4000, Belgium, 2001.
38. Martis, E.L., "Flow Regime Transitions in Bubble Column Reactors", August, 2004.
39. Massimilla, L., Solimando, A., and Squillace, E., British Chemical Engineering, April, 233, 1961.
40. Miron, A. S., Gomez, A. C., Camacho, F. G., Grima, E. M., and Chisti, Y., "Comparative evaluation of compact photobioreactors for large-scale monoculture of microalgae" Journal of Biotechnology. 70: 249-270, 1999.
41. Miron, A. S., Camacho, F. G., Gomez, A. C., Grima, E. M., and Chisti, Y. "Bubble- Column and Airlift Photobioreactors for Algal Culture" American Institute of Chemical Engineers Journal. 46(9): 1872-1887, 2000.
42. Mouza, K., A., Kazakis, N., A., and Paras, S., V., "Bubble Column Reactor Design Using CFD Code", Laboratory of Chem. Process and Plant Design Department of Chem. Eng. Aristotle University of Thessaloniki, 2004.
43. Nenes, A., Assimacopoulos, D., Markatos, N., and Mtsoulis, E., "Simulation of Airlift Pumps for Deep Water Wells", 1994.

44. Nguyen, K., Dawb, C.S., Chakkaa, P., Chenga, M., Brunsa, D.D., Finneya, C.E.A., Kennela, M.B., " Spatio-temporal dynamics in a train of rising bubbles", Chemical Engineering Journal **64**:1, 191-197, 1996.
45. Niels, G., Deen¹, Esther I.V. van den Hengel^{1,2}, Martin van Sint Annaland¹ and J.(Hans)A.M. Kuipers¹, " Multi-Scale Modeling of Dispersed Gas-Liquid Two-Phase Flows ", 5th International Conference on Multiphase Flow, ICMF'04 Yokohama, Japan, May 30–June 4, Paper No. K07, 2004.
46. Olmos, E., Gentric, C., Vial, Ch., Wild, G., and Midoux, N., "Numerical simulation of multiphase flow in bubble column reactors. Influence of bubble coalescence and break-up", Chemical Engineering Science, Vol. 56, pp. 6359-6365, 2001.
47. Olivieri, G., Marzocchella, A., Salatino, P., "Hydrodynamics of A Lab-Scale Two-Phase Internal Loop Airlift Reactor", Dip. di Ingegneria Chimica – Università degli Studi di Napoli Federico P.le Tecchio, 80 – 80125 Napoli, Italy , 2006.
48. Poulsen B. R., and Iversen, J. J. L., "Characterization of Gas Transfer and Mixing in a Bubble Column Equipped with a Rubber Membrane Diffuser" Biotechnology and Bioengineering. 58: 633-641, 1998.
49. Prince, M.J., and Blanch, H.W., "Bubble Coalescence and Break-up in Air-Sparged Bubble Columns", AIChE J., Vol 36, No 10, pp 1485-1499, 1990.

50. [http://www.Process technology computational fluid dynamics at BHRsolutions.htm](http://www.Process%20technology%20computational%20fluid%20dynamics%20at%20BHRsolutions.htm)
51. Ruzicka, M. C.; Zahradnik, J.; Drahos, J.; Thomas, N. H., "Homogeneous-heterogeneous regime transition in bubble columns. Chemical Engineering Science, 56(15), 4609-4626, (2001).
52. Sa'nchez Miro'n, A., Contreras Go'mez, A., Garc'a Camacho, F., Molina Grima, E. and Chisti, Y., 1999, Comparative evaluation of compact photobioreactors for large-scale monoculture of microalgae, J Biotechnol, 70: 249–270.
53. Sa'nchez Miro'n, A., Garc'a Camacho, F., Contreras Go'mez, A., Molina Grima, E. and Chisti, Y., 2000, Bubble column and airlift photobioreactors for algal culture, AIChE J, 46: 1872–1887.
54. Sarrafi, Amir; Jamialahmadi, Mohammad; Muller-Steinhagen, Hans; Smith, John M., "Gas holdup in homogeneous and heterogeneous gas-liquid bubble column reactors. Canadian Journal of Chemical Engineering, 77(1), 11-21, 1999.
55. Shun and Yasuhiro, "Gas-phase dispersion in bubble columns ", Chem. Eng. Science, Vol.45, No. 4, pp.901-905, 1990.
56. Shaikh, A., and Al-Dahhan, M., H., "A Review on Flow Regime Transition in Bubble Columns", International journal of chemical reactor engineering, Vol. 5, Review R1, 2007.

- 57.Silva, R., Neto1, S., and Vilar, E., "A Computational Fluid Dynamics Study of Hydrogen Bubbles in an Electrochemical Reactor", Brazilian Archives of Biology and Technology Journal, Vol.48, Special n.: pp. 219-229, June 2005.
- 58.Simon Lo," Application of Population Balance to CFD Modeling of Gas-Liquid Reactors", Trends in Numerical and Physical Modeling for Industrial Multiphase Flow, 2000.
- 59.Solbakken, T., and Hjertager, B., H., "A Computational and Experimental Study of Flow Pattern in a pilot and Full Scale Bubble Column", Third International Conference On Multiphase Flow, ICMF'98 Lyon, France, June 8-12, 1998.
- 60.Taitel, Y., D. Bornea and A.E. Buckler, "Modelling Flow Pattern Transitions for Steady Upward Gas-Liquid Flow in Vertical Tubes", AIChE J. **26**, 345-354, 1980.
- 61.Tharat, B. N. ; Shevad, A. V.; Bhilegaovkar, K. V.; Aglawe, R. H.; Parasu, U.; Thakre, S. S.; Pandit, A. B.; Sawant, S. B.; and Joshi, J. B., "Effect of sparger design and height to diameter ratio on fractional gas holdup in bubble column ", Trans. I. Chem., vol. 76, part A,October,1998.
- 62.Urseanu M. L. and Krishna, R., "Scaling up Bubble Column Reactors" Unpublished Ph.D. Thesis. Amsterdam, The Netherlands.: University of Amsterdam, Department of Chemical Engineering, 2000.

63. Vatai, GY., and Tekic, M.N., "Gas-Holdup and Mass Transfer in Bubble Columns with Pseudo Plastic Liquids", *Chem. Eng. Science*, Vol. 44, No. 10, pp. 2402-2407, 1989.
64. Viswanathan, K., Rao, S., D., "Circulation in bubble columns", *Chem. Eng. Science*, Vol. 38, No.3, pp. 474-478, 1983.
65. Vladimir and Andrei, "CFD Modeling of Gas-Liquid Flows in Water Electrolysis Units", Stuart Energy Systems Corporation 5101 Orbitor Drive, Mississauga ON L4W 4V1, CANADA, 2003.
66. Wallis, G. B., "One Dimensional Two Phase Flow", McGraw Hill, New York, 1969.
67. Wang, B., Rehm, W., Jülich, F., "Overview of Models for Multifluid /Multiphase Flows Based on CFD Codes D3UNS, CFX-5, IFSAS with Test Cases for Complex Flows (Part -2)", Forschungszentrum Jülich, Germany, 2003.
68. Wild, G., Li, H.Z., Poncin, S., and Olmos, E., "Some Aspects of the Hydrodynamics of Bubble Columns", *International Journal of Chem. Reactor Eng.*, Vol. 1, pp. 1-36, 2003.
69. Wilkinson, Peter M.; Spek, Arie P.; Van Dierendonck, Laurent L., "Design parameters estimation for scaleup of high-pressure bubble columns" *AIChE Journal*, 38(4), 544-54, 1992.

70. Wouter, "Splendid science", Harteveld - Department of Multi-Scale Physics, 2006.

APPENDIX "A"

1. Mathematical models

Governing equations

the governing equations will describe for the CFD calculations performed in this research. The multi-fluid model section describes the general formulation of the model equations. The multi fluid model will be used to setup Euler-Euler simulations.

Multi-fluid model

The general scalar advection-diffusion equation:

$$\frac{\partial}{\partial t} \varepsilon_{\alpha} \rho_{\alpha} \phi_{\alpha} + \nabla \cdot (\varepsilon_{\alpha} (\rho_{\alpha} U_{\alpha} \phi_{\alpha} - \Gamma_{\alpha} \nabla \phi_{\alpha})) = \varepsilon_{\alpha} S_{\alpha} + \sum_{\beta=1}^{N_p} c_{\alpha\beta} (\phi_{\beta} - \phi_{\alpha}) \quad \dots (1)$$

where α gas phase, β liquid phase.

For momentum equations this takes the form:

$$\begin{aligned} & \frac{\partial}{\partial t} \varepsilon_{\alpha} \rho_{\alpha} U_{\alpha} + \nabla \cdot (\varepsilon_{\alpha} (\rho_{\alpha} U_{\alpha} \otimes U_{\alpha} - \mu_{\alpha} (\nabla U_{\alpha} + (\nabla U_{\alpha})^T))) \\ & = \varepsilon_{\alpha} (B - \nabla p_{\alpha}) + \sum_{\beta=1}^{N_p} c_{\alpha\beta}^{(d)} (U_{\beta} - U_{\alpha}) \end{aligned} \quad \dots (2)$$

The continuity equation:

$$\frac{\partial}{\partial t} (\varepsilon_{\alpha} \rho_{\alpha}) + \nabla \cdot (\varepsilon_{\alpha} \rho_{\alpha} U_{\alpha}) = 0 \quad \dots (3)$$

And

$$\sum_{\alpha=1}^{N_p} \varepsilon_{\alpha} = 1 \quad \dots (4)$$

The formulas above define $4 N_p + 1$ equations for the following $5N_p$ unknowns: $U_\alpha, V_\alpha, W_\alpha, p_\alpha, \varepsilon_\alpha$. For this system of equations to be solved, $5N_p - 1$ more equations need to be added. In this research, the additional equation defines that all phases share the same pressure field:

$$p_\alpha = p_\beta = \dots = p \quad \dots (5)$$

Any additional quantities to be solved, such as tracer concentrations, take the general form of the advection diffusion equation, without interphase transfer terms $c_{\alpha\beta}$.

Turbulence models

In this research the general single phase $k-\varepsilon$ model, extended for the use in multi-phase systems, has been used. In this model, the effective viscosity in the momentum equations is the sum of the molecular and a turbulent viscosity:

$$\mu_{\alpha, eff} = \mu_\alpha + \mu_{T\alpha} \quad \dots (6)$$

With:

$$\mu_{T\alpha} = C_\mu \rho_\alpha \frac{k_\alpha^2}{\varepsilon_\alpha} \quad \dots (7)$$

Here, k represents the kinetic energy and ε represent the rate of turbulence dissipation. The volume fraction equation is modified in the following way:

$$\frac{\partial}{\partial t}(\varepsilon_\alpha \rho_\alpha) + \nabla \cdot (\varepsilon_\alpha \rho_\alpha U_\alpha - \Gamma \nabla \varepsilon_\alpha) = 0 \quad \dots (8)$$

With:

$$\Gamma_\alpha = \frac{\mu_{T\alpha}}{\sigma_\alpha} \quad \dots (9)$$

The transport equations for k and ε :

$$\frac{\partial}{\partial t} \varepsilon_\alpha \rho_\alpha k_\alpha + \nabla \cdot \left(\varepsilon_\alpha \left(\rho_\alpha U_\alpha k_\alpha - \left(\mu_\alpha + \frac{\mu_{T\alpha}}{\sigma_\alpha} \right) \nabla k_\alpha \right) \right) = \varepsilon_\alpha S_{k\alpha} + \sum_{\beta=1}^{N_p} c_{\alpha\beta}^{(k)} (k_\beta - k_\alpha) \quad \dots (10)$$

With:

$$S_{k\alpha} = P_\alpha + G_\alpha - \rho_\alpha \varepsilon_\alpha \quad \dots (11)$$

$$S_{\varepsilon\alpha} = \frac{\varepsilon_\alpha}{k_\alpha} (C_{1\varepsilon} (P_\alpha + C_{3\varepsilon} \max(G_\alpha, 0)) - C_{2\varepsilon} \rho_\alpha \varepsilon_\alpha) \quad \dots (12)$$

In which shear production P and production due to body forces G for incompressible flows are given by:

$$P = \mu_{eff} \nabla U \cdot (\nabla U + (\nabla U)^T) \quad \dots (13)$$

$$G = 0 \quad \dots (14)$$

The ~~ke~~ model has the following model parameters: C_μ , $C_{1\varepsilon}$, $C_{2\varepsilon}$, $C_{3\varepsilon}$. In addition, the Prandtl numbers σ_α for the various quantities need to be specified.

Interphase transport terms

In this research, transport between the phases is only taken into account for momentum.

Drag

Drag models defines how momentum is being transferred if a difference in velocity is present between two phases. In the multi-fluid model, interphase momentum transfer can be modeled by specifying a value for the interphase momentum transfer coefficients $c_{\alpha\beta}^{(d)}$ equation (1).

Particle model

The particle model models the interphase momentum transfer between a continuous phase α and a disperse phase β :

$$c_{\alpha\beta}^{(d)} = \frac{3}{4} \frac{C_D}{d} \varepsilon_\beta \rho_\alpha |U_\beta - U_\alpha| \quad \dots \quad (15)$$

$$|U_\beta - U_\alpha| = \sqrt{(U_{x,\beta} - U_{x,\alpha})^2 + (U_{y,\beta} - U_{y,\alpha})^2 + (U_{z,\beta} - U_{z,\alpha})^2} \quad \dots \quad (16)$$

Or, alternatively (only if explicitly mentioned), a modification of equation (15) that takes into account the holdup of the continuous phase:

$$c_{\alpha\beta}^{(d)} = \frac{3}{4} \frac{C_D}{d_p} \varepsilon_\beta \varepsilon_\alpha \rho_\alpha |U_\beta - U_\alpha| \quad \dots \quad (17)$$

In the above, the drag coefficient C_D is a model parameter, and d represents the average size of the particles or bubbles that make up phase β .

2. Euler-Euler

In Euler-Euler simulations, separate phases are treated as interpenetrating fluids. This means that at a certain position, all phases can be present with a certain volume fraction, and no clear interface between the phases can be established. This allows both the length and the time scale on which these equations are being solved to be larger than in DNS methods.

The equations governing Euler-Euler simulations are the equations of the multi-fluid model (equation 1 to 5). The only body force taken into account in this research is gravitational force:

$$B_\alpha = \rho_\alpha g \quad \dots \quad (18)$$

Drag

In this research, the drag coefficient C_D is based on the distorted flow regime (the intermediate regime between spherical bubbles and spherical cap bubbles):

$$C_D = \left(\frac{2}{3}\right) E_o^{1/2} \quad \dots \quad (19)$$

With:

$$E_o = g \Delta \rho d_b^2 / \sigma \quad \dots \quad (20)$$

Turbulence

There is no turbulence modeling for the discontinuous (gas) phase. For the continuous phase (liquid), the general multi phase k_ϵ model is being applied (equations 6-14). The interphase transfer coefficients $C_{\alpha\beta}^{(k)}$ and $C_{\alpha\beta}^{(\epsilon)}$ are taken to be zero. The Prandtl numbers σ for the various quantities are not being used, resulting in the eddy diffusion coefficients Γ for the various transported quantities to be zero. For the other parameters in the k_ϵ model, the default values are being used, as shown in table 1:

Table 1: Model constants in k_ϵ model

model constant	default value
C_μ	0.09
$C_{1\epsilon}$	1.44
$C_{2\epsilon}$	1.92
$C_{3\epsilon}$	0

APPENDIX "B"

Table (A-1) Physical properties used in CFD simulation

property	water	air
Density [kg/m ³]	998	1.3
Viscosity [Pa.s]	1x10 ⁻³	17x10 ⁻⁶
Surface tension [N/m]	0.073	

Table (A-2) Experimental data of airlift reactor of Van Baten et. al. (2003)

RISER			DOWNCOMER
Superficial gas velocity (m/s)	Gas holdup (-)	Liquid velocity (m/s)	Liquid velocity (m/s)
0.0153	0.022301	0.358	0.4
0.019125	0.027684	0.43316	0.48
0.02371	0.032298	0.428991	0.5
0.035955	0.045371	0.52916	0.6
0.04972	0.056906	0.5789	0.68
0.07191	0.073824	0.75	0.835
0.0933	0.08459	0.77469	0.865
0.118575	0.098432	0.884	1.02

Table (A-3) Simulation results of airlift reactor

RISER			DOWNCOMER
Superficial gas velocity (m/s)	Gas holdup (-)	Liquid velocity (m/s)	Liquid velocity (m/s)
0.018634	0.024274	0.482885	0.335041
0.040887	0.049175	0.553024	0.50652
0.056583	0.063877	0.652325	0.578915
0.081263	0.078823	0.727244	0.736721
0.094986	0.086404	0.842264	0.682285
0.114192	0.085158	0.77874	0.787402

Table (A-4) Radial distribution of gas holdup and liquid velocity in riser and down comer at 0.018634 m/s superficial gas velocity.

Radial distributions (m)	Liquid velocity (m/s)	Gas holdup (-)
0.01	0.392218	0.017798
0.02	0.38143	0.017798
0.03	0.381402	0.017797
0.04	0.372063	0.017794
0.046	0.362946	0.017787
0.049	0.3619	—
0.059	-0.35983	—
0.0645	-0.36434	—
0.07	-0.3621	—

Table (A-5) Radial distribution of gas holdup and liquid velocity in riser and down comer at 0.040887 m/s superficial gas velocity.

Radial distributions (m)	Liquid velocity (m/s)	Gas holdup (-)
0.01	0.516938	0.029522
0.02	0.503818	0.029522
0.03	0.503784	0.02952
0.04	0.492426	0.029513
0.046	0.481306	0.029498
0.049	0.481	—
0.059	-0.4775	—
0.0645	-0.47577	—
0.07	-0.47286	—

Table (A-6) Radial distribution of gas holdup and liquid velocity in riser and down comer at 0.056583 m/s superficial gas velocity.

Radial distributions (m)	Liquid velocity (m/s)	Gas holdup (-)
0.01	0.608003	0.039515
0.02	0.593267	0.039515
0.03	0.59323	0.039513
0.04	0.580473	0.039502
0.046	0.567973	0.039479
0.049	0.5659	—
0.059	-0.5637	—
0.0645	-0.55465	—
0.07	-0.55123	—

Table (A-7) Radial distribution of gas holdup and liquid velocity in riser and down comer at 0.081263 m/s superficial gas velocity.

Radial distributions (m)	Liquid velocity (m/s)	Gas holdup (-)
0.01	0.675265	0.047486
0.02	0.6594	0.047486
0.03	0.65936	0.047482
0.04	0.645626	0.047468
0.046	0.632164	0.047439
0.049	0.63	—
0.059	-0.62756	—
0.0645	-0.61047	—
0.07	-0.60672	—

Table (A-8) Radial distribution of gas holdup and liquid velocity in riser and down comer at 0.094986 m/s superficial gas velocity.

Radial distributions (m)	Liquid velocity (m/s)	Gas holdup (-)
0.01	0.744339	0.056626
0.02	0.72735	0.056625
0.03	0.727306	0.05662
0.04	0.712602	0.056601
0.046	0.698162	0.056564
0.049	0.697	—
0.059	-0.69323	—
0.0645	-0.66799	—
0.07	-0.66392	—

Table (A-9) Radial distribution of gas holdup and liquid velocity in riser and down comer at 0.11419193 m/s superficial gas velocity.

Radial distributions (m)	Liquid velocity (m/s)	Gas holdup (-)
0.01	0.801456	0.064221
0.02	0.783558	0.06422
0.03	0.783513	0.064215
0.04	0.768022	0.064192
0.046	0.747524	0.064145
0.049	0.7474	—
0.059	-0.74764	—
0.0645	-0.71396	—
0.07	-0.70961	—

Table (A-10) The relation between the drift-flux and the gas holdup

Superficial gas velocity (m/s)	Gas holdup (-)	Drift flux (m/s)
0.018634	0.024274	0.018182
0.040887	0.049175	0.038876
0.056583	0.063877	0.052969
0.081263	0.078823	0.074858
0.094986	0.086404	0.086779
0.11419193	0.085158	0.104468

Table (A-11) Local and average gas holdup and liquid velocity in bubble column reactor at superficial gas velocity 0.001357 m/s.

Z	Gas holdup (-)	Liquid velocity (m/s)
0.1	0.00707348	0.0795419
1	0.00422481	0.0137103
1.8	0.00432732	0.0101247
AVG.	0.005209	0.034459

Table (A-13) Local and average gas holdup and liquid velocity in bubble column reactor at superficial gas velocity 0.007683 m/s.

Z	Gas holdup (-)	Liquid velocity (m/s)
0.1	0.0332421	0.165354
1	0.0223437	0.00533512
1.8	0.0223916	0.00388122
AVG.	0.025992	0.05819

Table (A-14) Local and average gas holdup and liquid velocity in bubble column reactor at superficial gas velocity 0.015772 m/s.

Z	Gas holdup (-)	Liquid velocity (m/s)
0.1	0.0613934	0.219588
1	0.0447598	0.00074594
1.8	0.0447268	0.00156284
AVG.	0.050293	0.073966

Table (A-15) Local and average gas holdup and liquid velocity in bubble column reactor at superficial gas velocity 0.031988 m/s.

Z	Gas holdup (-)	Liquid velocity (m/s)
0.1	0.112595	0.286737
1	0.0940834	0.00448284
1.8	0.0942913	0.00494149
AVG.	0.100323	0.09872

APPENDIX C

ANSYS PROGRAMING

Modify	Set the following				
ANSYS launch product	Mechanic al U	file	select	run	
progress	Element type	add	200	ok	
	option	tetra	ok		
modeling	volume	cylinder	partial	X=0, Y=0	apply
				θ1=0,Ri=0	
				θ2=30, Ro=0.0735	
				Depth=1.71	
Work plane	Offset by increment	(0,0,1.71)	Ok		
modeling	volume	cylinder	partial	X=0,y=0	apply
				Ri=0, θ1=0	
				Ro=0.147, θ2=30	
				Depth=0.5	
Work plane	Offset by increment	(0,0,0.0123)	Ok		
modeling	volume	cylinder	partial	X=0,y=0	apply
				Ri=0.053, θ1=0	
				Ro=0.059, θ2=30	
				Depth=1.71	
operate	blooders	add	volume	Select outside cylinders	ok

operate	blooders	sustract	volume	Select outside cylinder		ok
				Select inside cylinder		ok
modeling	volume	con	Rb=0.0378, z1=0.0123, θ1=0	Rt=0.0735, z2=-0.048, θ2=30		apply
Work plane	Offset by increment	(0,0,-0.046)	Ok			
modeling	volume	cylinder	hallow	X=0.01,y=0.0025		ok
				di=0, θ1=0		
				do=0.00025, θ2=30		
				Depth=-0.001		
modeling	volume	cylinder	hallow	X=0.005,y=0.0015		ok
				di=0, θ1=0		
				do=0.00025, θ2=30		
				Depth=-0.001		
operate	blooders	sustract	volume	Select large cone		Ok
				Select small cone		ok
operate	boolders	volume	Pick all			
	meshing	Mesh interrupt	dauft	Select the first		ok
	Mesh tool	area	Select 5	area	mesh	Pick all
	select	1 choice	area	By pick	From full	apply
	select	sparger	ok			
element	attach	area	reselect	ok		
select	manger	create	element	Write sparger		ok
Select	every thing					

Repeat the last three step for (top, sym1, sym2, dti, dro), Then:

select	1 choice	volume	By pick	From full	apply	pick all
element	attach	volume	reselect	ok		
select	manger	create	element	Write dom.	ok	
Select	every thing					
Select	manger	Create assembly				
achieves	write	all	cdb	ok		

Creating a New Simulation

Click on CFX-5 (Pre-CFX)

1. Create a new simulation named *Bubble Column* using General Mode.

Importing the Mesh

1. Click Import Mesh.
2. Apply the following settings

Modify	Set the following	To this value
Definition	File	Bubble Column Mesh.gtm

3. Click OK.

Creating the Domain

1. Create a new domain named *Bubble Column*.
2. Apply the following settings

General Options	Basic Settings > Location		Assembly
	Fluids List		Air at 25 C, Water
	Domain Models > Pressure > Reference Pressure		0 [Pa]
	Domain Models > Buoyancy > Option		Buoyant
	Domain Models > Buoyancy > Gravity X Dirn.		0 [m s ⁻²]
	Domain Models > Buoyancy > Gravity Y Dirn.		0 [m s ⁻²]
	Domain Models > Buoyancy > Gravity Z Dirn.		-9.81 [m s ⁻²]
	Domain Models > Buoyancy > Buoy. Ref. Density*		998 [kg m ⁻³]
Fluid Details	Fluid Details > Air at 25 C		Select
	Fluid Details > Air at 25 C > Morphology > Option		Dispersed

		Fluid
	Fluid Details > Air at 25 C > Morphology > Mean Diameter	5 [mm]
Fluid Pairs	Fluid Pairs > Air at 25 C Water > Surface Tension Coefficient	Select
	Fluid Pairs > Air at 25 C Water > Surface Tension Coefficient > Surf. Tension Coeff	0.073 [N m ⁻¹] [†]
	Fluid Pairs > Air at 25 C Water > Momentum Transfer > Drag Force > Option	Ishii Zuber
	Fluid Pairs > Air at 25 C Water > Momentum Transfer > Drag Force > Volume Fraction Correction Exponent	Select
	Fluid Pairs > Air at 25 C Water > Momentum Transfer > Non-drag Forces > Turbulent Dispersion Force > Option	Lopez de Bertodano
	Fluid Pairs > Air at 25 C Water > Momentum Transfer > Non-drag Forces > Turbulent Dispersion Force > Dispersion Coeff.	0.3
	Fluid Pairs > Air at 25 C Water > Turbulence Transfer > Option	Sato Enhanced Eddy Viscosity

*. For dilute dispersed multiphase flow, always set the buoyancy reference density to that for continuous fluid. For details, see *Buoyancy*

[†]. This must be set to allow the Grace Drag model to be used.

3. Click OK.

Creating the Boundary Conditions

For this simulation of the airlift reactor, the boundary conditions required are:

- An inlet for air on the sparger.
- A degassing outlet for air at the liquid surface.
- A thin surface wall for the draft tube.
- An exterior wall for the outer wall, base and sparger tube.
- Symmetry planes for the cross sections.

Inlet Boundary There is an infinite number of inlet velocity/volume fraction combinations that will produce the same mass inflow of air. The combination chosen gives an air inlet velocity close to the terminal rise velocity. Since the

water inlet velocity is zero, you can adjust its volume fraction until the required mass flow rate of air is obtained for a given air inlet velocity.

1. Create a new boundary condition named *Sparger*.

2. Apply the following settings

Modify	Set the following	To this value
Basic Settings	Boundary Type	Inlet
	Location	Sparger
Fluid Values	Boundary Conditions > Air at 25 C	Select
	Boundary Conditions > Air at 25 C > Velocity > Normal Speed	0.06 [m s ⁻¹]
	Boundary Conditions > Air at 25 C > Volume Fraction > Volume Fraction	1
	Boundary Conditions > Water	Select
	Boundary Conditions > Water > Velocity > Normal Speed	0 [m s ⁻¹]
	Boundary Conditions > Water > Volume Fraction > Volume Fraction	0
	tensity	5%

3. Click OK

Outlet Boundary

The top of the reactor will be a degassing boundary, which is classified as an outlet boundary.

1. Create a new boundary condition named *Top*.

2. Apply the following settings.

Modify	Set the following	To this value
Basic Settings	Boundary Type	Outlet
	Location	Top
Boundary Details	Mass and Momentum > Option	Degassing Condition*

3. Click OK

Thin Surface Draft Tube Boundary

Thin surfaces are created by specifying a wall boundary condition on *both* sides of an internal region. If only one side has a boundary condition then the

ANSYS CFX-Solver will fail. To assist with this, you can select only one side of a thin surface and then enable Create Thin Surface Partner toggle. ANSYS CFX-Pre will then try to automatically create another boundary condition for the other side.

1. Create a new boundary condition named *DraftTube*.
2. Apply the following settings

Modify	Set the following	To this value
Basic Settings	Boundary Type	Wall
	Location	Draft Tube
	Create Thin Surface Partner	Select
Fluid Values	Boundary Conditions > Air at 25 C	Select
	Boundary Conditions > Air at 25 C > Wall Influence On Flow > Option	No Slip
	Boundary Conditions > Water	Select
	Boundary Conditions > Water > Wall Influence On Flow > Option	No Slip

3. Click OK.

A boundary condition named Draft Tube Other Side will now be created automatically.

Symmetry Plane Boundary

In this step you will create symmetry plane boundary conditions on the Symmetry1 and Symmetry2 locators, one for each of the two vertical cross sections of the reactor sector.

1. Create a new boundary condition named *SymP1*.
2. Apply the following settings

Modify	Set the following	To this value
Basic Settings	Boundary Type	Symmetry
	Location	Symmetry1

3. Click OK.

4. Create a new boundary condition named *SymP2*

5. Apply the following settings

Modify	Set the following	To this value
Basic Settings	Boundary Type	Symmetry
	Location	Symmetry2

6. Click OK.

Modifying the Default Boundary

The remaining external regions are assigned to the default wall boundary condition. This needs to be modified to set the Air phase to Free Slip.

1. In the Physics tab, under Flow, in Bubble Column, edit Bubble Column Default.

2. Apply the following settings.

Modify	Set the following	To this value
Fluid Values	Boundary Conditions > Air at 25 C	Select
	Boundary Conditions > Air at 25 C > Wall	No slip
	Influence on Flow > Option	

3. Click OK.

The boundary condition specifications are now complete.

Setting Initial Values

It often helps to set an initial velocity for a dispersed phase that is different to that of the continuous phase. This results in a non-zero drag between the phases which can help stability at the start of a simulation.

For some bubble column problems, improved convergence can be obtained by using CEL (CFX Expression Language) to specify a non zero volume fraction, for air in the riser and a zero value in the downcomer. This should be done if two solutions are possible (for example, if the flow could go up the downcomer and down the riser).

Additional information on setting initial conditions in a multiphase simulation is available.

1. Click Global Initialisation.

Since a single pressure field exists for a multiphase calculation you do not set pressure values on a per fluid basis.

2. Apply the following settings

Modify	Set the following	To this value
Fluid Settings	Fluid Specific Initialisation > Air at 25 C	Select
	Fluid Specific Initialisation > Air at 25 C > Initial Conditions > Cylindrical Velocity Components > Option	Automatic with Value
	Fluid Specific Initialisation > Air at 25 C > Initial Conditions > Cylindrical Velocity Components > Axial	0 [m s ⁻¹]
	Fluid Specific Initialisation > Air at 25 C > Initial Conditions > Cylindrical Velocity Components > Radial	0.06 [m s ⁻¹]
	Fluid Specific Initialisation > Air at 25 C > Initial Conditions > Cylindrical Velocity Components > Theta	90 [m s ⁻¹]
	Fluid Specific Initialisation > Water	Select*
	Fluid Specific Initialisation > Water > Initial Conditions > Cartesian Velocity Components > Option	Automatic with Value
	Fluid Specific Initialisation > Water > Initial Conditions > Cartesian Velocity Components > U	0 [m s ⁻¹]
	Fluid Specific Initialisation > Water > Initial Conditions > Cartesian Velocity Components > V	0 [m s ⁻¹]
	Fluid Specific Initialisation > Water > Initial Conditions > Cartesian Velocity Components > W	0 [m s ⁻¹]
	Fluid Specific Initialisation > Water > Initial Conditions > Turbulence Kinetic Energy > Option	Automatic
	Fluid Specific Initialisation > Water > Initial Conditions > Turbulence Eddy Dissipation	Select
	Fluid Specific Initialisation > Water > Initial Conditions > Turbulence Eddy Dissipation > Option	Automatic
	Fluid Specific Initialisation > Water > Initial Conditions > Volume Fraction > Option	Automatic with Value
	Fluid Specific Initialisation > Water > Initial Conditions > Volume Fraction > Volume Fraction	1†

3. Click OK

Setting Solver Control

If you are using a maximum edge length of 0.005 m or less to produce a finer mesh, we recommend using a Target Residual of $1.0E-05$ to obtain a more accurate solution.

1. Click Solver Control.
2. Apply the following settings

Modify	Set the following	To this value
Basic Settings	Convergence Control > Timescale Control	Physical Timescale
	Convergence Control > Physical Timescale	1 [s]

3. Click OK.

Writing the Solver (.def) File

1. Click Write Solver File.
2. Apply the following settings

Set the following	To this value
Filename	BubbleColumn.def
Operation	Start Solver Manager
Quit CFX-Pre	Select

*. If using ANSYS CFX-Pre in Standalone Mode.

3. Click OK.
4. Quit ANSYS CFX-Pre, saving the simulation (.cfx) file at your discretion.

Obtaining a Solution using ANSYS CFX-Solver Manager

The ANSYS CFX-Solver Manager will be launched after ANSYS CFX-Pre has closed down. You will be able to obtain a solution to the CFD problem by following the instructions below.

Note: If a fine mesh is used for a formal quantitative analysis of the flow in the reactor, the solution time will be significantly longer than for the coarse mesh. You can run the simulation in parallel to reduce the solution time.

1. Ensure Define Run is displayed.

2. Click Start Run.

ANSYS CFX-Solver runs and attempts to obtain a solution. This can take a long time depending on your system. Eventually a dialog box is displayed.

3. Click OK.

4. Click Post–Process Results.

5. If using ANSYS CFX-Solver in Standalone Mode, select Shut down Solver Manager, and then click OK.

Viewing Results in ANSYS CFX-Post

Coarse Mesh Results

Because the simulation in this tutorial is conducted on a coarse grid, the results are only suitable for a qualitative demonstration of the multiphase capability of ANSYS CFX, Release 10.0. You will first examine the distribution of velocities and fluid volume fraction by creating the following plots. The results will then be verified to check if the values are reasonable.

1. Select View Towards -Z.
2. Zoom in as required.
3. Turn on the visibility of SymP1.
4. Apply the following settings to SymP1.

Modify	Set the following	To this value
Color	Mode	Variable
	Variable	Air at 25 C.Volume Fraction
	Range	Range User Specified
	Min	0
	Max	0.025

Displaying the Entire Airlift Reactor Geometry

Display the entire airlift reactor geometry by expanding the View Control object and double-clicking the Default Transform object:

1. In the Objects tab, under View Control, edit Default Transform.
2. Apply the following settings

Modify	Set the following	To this value
Definition	Instancing Info From Domain	Clear
	of Copies	12
	Apply Rotation > Axis	Y
	Apply Rotation > # of Passages	12

3. Click Apply

شكر وتقدير

في البداية اشكر الله عز وجل الذي وفقني لاكمال متطلبات هذا البحث. وانا انهي بحثي لا يسعني واعترافا بالفضل الا ان اتقدم بوافر الشكر والامتنان للاستاذ المشرف الدكتور نصير عبود الحبوبى لاقتراحه موضوع الرسالة واشرافه عليها ولمواصلته ومتابعته العلمية للبحث وما ترتب على ذلك من توجيهات قيمه واراء سديدة.

كما اتقدم بجزيل الشكر الى رئيس قسم الهندسة الكيماوية، و جميع اساتذة قسم الهندسة الكيماوية لمساعدتهم القيمة لي طيلة فترة الدراسة ولمدهم يد العون لي خلال اعداد هذه الرسالة. واتقدم بشكري وامتناني الى عمادة جامعة النهرين/كلية الهندسة ،لمساعدتهم ودعمهم الدائم لي طيلة فترة الدراسة.

وشكري الجزيل الى جميع زملائي و زميلاتي الذين مدو يد العون عند حاجتي اليها في البحث.

ولا انسى ان اتقدم بجزيل الشكر والتقدير الى من ساندني وساعدني على تخطي الصعوبات خلال فترة البحث الى الذين لا مثيل لهم في الدنيا الى أمي العزيزة ، أخوتي وأخواتي.

م. رنا رسول الحصرى

الخلاصة

تتعامل محاكاة ديناميكية السوائل الحسابية (CFD) مع حلّ المعادلات الديناميكية السائلة على الحواسيب الإلكترونية، وهذا يتطلبُ نسبياً بضْعَ فرضياتٍ تقديرية وتعطي وصفاً تاماً لهيدروديناميكية الأعمدة الفقاعية. أن التنبؤ التفصيلي للجريان، يعطى صورة دقيقة لسلوك السائل .

تم استخدام محاكاة ديناميكية السوائل الحسابية (CFD) ثلاثية الأبعاد باستخدام ANSYS مع نموذج Euler-Euler لقياس هايدروديناميكية العمود الفقاعي ذي أنبوب السحب ، ومقارنتها مع مثيلاتها من التجارب العملية التي اجراها العالم باتن- واخرين (1999) ، ومقارنتها أيضاً بهيدروديناميكية مفاعل عمود الفقاعة، يشتغل بنظام هواء / ماء في نظام تدفق الفقاعة المتجانس. لوحظ أن سرع دوران السائل متجانسة في العمود الفقاعي ذي أنبوب السحب عند مقارنتها مع مثيلاتها للعمود الفقاعي، وهذا يؤدي إلى انخفاض معامل احتجاز الغاز. في أنبوب السحب للعمود الفقاعي تكون حركة الغاز و السائل عملياً ضمن نطاق التدفق الكتلي، بينما في العمود الفقاعي، تتوزع سرعة الغاز و السائل بشكل قطعيّ مكافئ.

لوحظ في مفاعلات العمود الفقاعي ذي أنبوب السحب ظهور نظام الانتقال في سرع الغاز السطحية العالية بسبب قدرتها للاشتغال في نظام تدفق الفقاعة المتجانس حتى سرع غاز سطحية أعلى بكثير.

(2005)

1430

2009